RSC Advances

Design of a structural framework with potential use to develop balanced multifunctional agents against Alzheimer's disease

Journal:	*RSC Advances*
Manuscript ID:	RA-ART-09-2014-010692.R3
Article Type:	Paper
Date Submitted by the Author:	29-Nov-2014

Complete List of Authors:	Jiang, Neng; China Pharmaceutical University, Department of Natural Medicinal Chemistry Wang, Xiao-Bing; China Pharmaceutical University, Department of Natural Medicinal Chemistry Li, Zhong-Rui; China Pharmaceutical University, Department of Natural Medicinal Chemistry Li, Su-Yi; China Pharmaceutical University, Department of Natural Medicinal Chemistry Xie, Sai-Sai; China Pharmaceutical University, Department of Natural Medicinal Chemistry Huang, Ming; China Pharmaceutical University, Department of Natural Medicinal Chemistry Kong, Ling-Yi; China Pharmaceutical University, Department of Natural Medicinal Chemistry

Graphical abstract

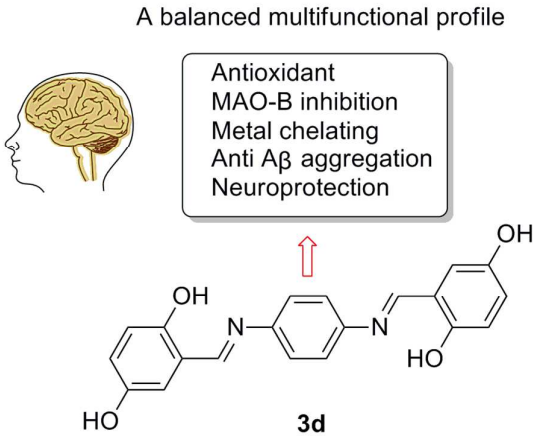

A series of small molecules had been designed, synthesized, and evaluated as multifunctional ligands against Alzheimer's disease (AD). Compound **3d** showed a balanced multifunctional profile covering anti-*β*-amyloid (A*β*) aggregation, antioxidant, monoamine oxidase B (MAO-B) inhibition, metal chelation, and neuroprotective properties at low micromolar concentrations.

Design of a structural framework with potential use to develop balanced multifunctional agents against Alzheimer's disease

Neng Jiang, Xiao-Bing Wang, Zhong-Rui Li, Su-Yi Li, Sai-Sai Xie, Ming Huang and Ling-Yi Kong*

State Key Laboratory of Natural Medicines, Department of Natural Medicinal Chemistry, China Pharmaceutical University, 24 Tong Jia Xiang, Nanjing 210009, People's Republic of China

* *Corresponding Author. Tel/Fax: +86-25-83271405; E-mail: cpu_lykong@126.com (Ling-Yi Kong);*

Abstract

A series of small molecules had been designed, synthesized, and evaluated as multifunctional ligands against Alzheimer's disease (AD). The results of biological activity tests showed that most of the molecules exhibited a significant ability to inhibit self-induced *β*-amyloid ($A\beta_{1\text{-}42}$) aggregation, and to function as potential antioxidants and biometal chelators. Among these compounds, compound **3d** was found to be highly potent and showed a balanced multifunctional profile covering inhibitory activity against self-induced $A\beta_{1\text{-}42}$ aggregation (IC_{50} = 7.8 μM), strong free radical scavenging activities [IC_{50} (ABTS) = 1.82 μM; IC_{50} (DPPH) = 15.4 μM] and inhibitory activity against MAO-B (IC_{50} = 6.4 μM). Moreover, it showed excellent metal chelating property and good inhibitory activity against Cu^{2+}-induced $A\beta_{1\text{-}42}$ aggregation, and was capable of decrease reactive oxygen species (ROS) induced by Cu^{2+}-$A\beta_{1\text{-}42}$. Importantly, compound **3d** was the most neuroprotective against neuronal death induced by oxidative stress and *β*-amyloid ($A\beta_{1\text{-}42}$), and was able to cross the blood–brain barrier (BBB), according to a parallel artificial membrane permeation assay. These results indicated that compound **3d** might be a promising lead compound for AD treatment.

1. Introduction

Alzheimer's disease (AD), the most common form of dementia associated with progressive loss of memory, speech, and recognition, occurs most frequently in elderly people.[1,2] It is believed that 35.6 million people suffered from AD in 2010 and that the number will double every 20 years, leading to more than 115 million people with AD in 2050.[3] The etiology of AD is still enigmatic, and some hallmarks, such as *β*-amyloid (A*β*) deposits, *τ*-protein aggregation, oxidative stress, inflammation, dyshomeostasis of biometals, neuronal death, and low levels of acetylcholine, are considered to play important roles in the pathogenesis of this disease.[4] In recent decades, much evidence has suggested that AD is a multifaceted illness. The "one-molecule, multiple-functionalities" paradigm is effective in treating complex diseases because of the ability of the drug to interact with multiple functionalities responsible for disease pathogenesis. Thus, a more appropriate approach to addressing the multifaceted nature of AD may be the development of multi-functionality-directed ligands.[5, 6]

A*β* plaques, widely accepted as the key pathological feature of AD, are mainly constituted by aggregation of the A*β* peptide, a 39- to 43-residue-long protein, derived from the amyloid precursor protein (APP).[7] Because A*β* is the main component of senile plaques, the "amyloid hypothesis" proposes that the production and accumulation of the oligomeric aggregates of A*β* in the brain are the central event in the pathogenesis of AD and these aggregates initiate the pathogenic cascade that ultimately leads to neuronal loss and dementia.[8] Furthermore, $A\beta_{1-42}$ aggregates into oligomers and fibrils in the brain and causes strong neuronal toxicity.[9] Prevention and clearance of A*β* aggregation in the brain is having neuroprotective effects and being considered as potential therapies for AD.

Recently, abundant data have indicated that excessive biometals, such as iron, zinc, and copper, exist in the brains of AD patients (Cu, ~400 μM; Zn and Fe, ~1 mM),[10,11] and it is several-fold to the normal age-matched neuropil (Cu,~70 μM; Zn,~350 μM; Fe,~340 μM).[11] *In vitro* experiments revealed that these metals are known to interact with A*β* peptides and promote their aggregation, which has been suggested to be

involved in neurotoxicity.[12-18] On the other hand, redox-active metal ions like Cu and Fe contribute to the production of reactive oxygen species (ROS) and widespread oxidation damages observed in AD brains.[19, 20] Therefore, the modulation of these biometals in the brain has been proposed to be a potential therapeutic strategy for the treatment of AD.[11]

Oxidative stress plays an important role in the pathogenesis of AD.[21] Neuronal tissue is very sensitive to oxidative stress, and an imbalance in pro-oxidant vs. antioxidant homeostasis in the CNS results in the production of several potentially toxic reactive oxygen species, which accelerate the progression of aging and aged-related neurodegenerative disorders.[22] Antioxidant protection is necessary during aging, especially in AD patients, because of the rapid decline of endogenous antioxidant protection. A recent statistical study involving developed countries indicated that a higher consumption of dietary antioxidants is associated with the lower rates of dementia.[23] Overall, oxidative stress could be attributed to a high degree of neurotoxicity leading to neuronal death and ultimately, cognitive impairment. Thus, the scavenging of ROS produced by such oxidation are important strategies for neuroprotective effects and preventing or slowing down the progression of aging and aged-related neurodegenerative disorders.

Monoamine oxidases A and B (MAO-A and MAO-B) are important FAD-dependent enzymes (flavoenzymes), localized on the mitochondrial outer membrane, which catalyze the oxidative deamination of biogenic amines and monoamine neurotransmitters. MAO-B exhibits higher affinity towards phenylethylamine (PEA) and benzylamine, and is potently inhibited by selegiline.[24-26] The reaction catalyzed by MAO results in the production of hydrogen peroxide (H_2O_2) and other reactive oxygen species, which may contribute to oxidative stress and cell damage.[27-29] Selegiline, a selective MAO-B inhibitor, has been shown to significantly improve learning and memory deficits in animal models associated with AD and to slow the disease progression in AD patients.[30] This evidence suggested that selective MAO-B inhibitors seem to be an important treatment of AD.

Overall, because of the involvement of numerous factors (e.g., metal-free/-associated

Aβ species, metals, free radicals, MAO-B) and their potential interconnection in AD pathogenesis, the causative agents in this multifaceted disease remain to be unambiguously identified. Evidence suggests that the most successful treatment strategy will likely incorporate a sequential, multifactorial approach.[6] Recently, multi-functional compounds targeting metal-induced Aβ aggregation have been extensively studied for AD treatments,[31-33] and our group has also reported the synthesis of tacrine–coumarin hybrids and (*E*)-*N*-benzylideneaniline derivatives as multi-functional agents against AD.[34-36] Inspired by this concept, curcumin which already showed broad spectrum of biological activities related to AD is selected as the lead compound.[37] Curcumin is a yellowish polyphenol compound isolated from turmeric which might be responsible for the low age-adjusted prevalence of AD in India.[37] As shown in Fig. 1, the structure of curcumin is similar to that of the IMSB (known Aβ imaging agent). They all have two aromatic end groups and a linker region in the middle.[38] It is referred that the two aromatic groups and their polar substitution are essential to their activities in terms of the efficient binding at the Aβ peptide guided π-stacking and hydrogen bond interactions.[39] For Aβ/metal−Aβ interactions, multifunctional ligand (**ML)** was constructed by combining two aromatic end groups of the curcumin or IMSB, two known Aβ imaging agents, with compounds **1** and **2**, two molecules previously reported to target and regulate metal−Aβ (Fig. 1). For metal chelation, we utilized the Schiff bases and phenolic hydroxyl groups as the chelators. These conjugates were designed to become trimers due to Cu^{2+} coordination, holding great promise for Cu^{2+} elimination and Aβ assembly inhibition abilities. For antioxidant activity, substituents (i.e., phenolic groups, Fig. 1)[40−42] known to have antioxidant capability were integrated into **ML**. Almost all structural elements were selected to adhere to values of Lipinski's rules and logBB for possible drug-likeness and BBB penetration (Table 1).[43-46]

In this paper, we described here the design, synthesis and pharmacological evaluation of a series of small molecules as multifunctional anti-AD agents. The pharmacological evaluations of these compounds included the inhibition of self-induced and Cu^{2+}-induced Aβ aggregation, antioxidant, inhibition of MAO-B

activity, metal chelation, ROS induced by Cu^{2+}-Aβ, neuroprotective properties against oxidative toxicity and Aβ toxicity, and the blood-brain barrier.

2. Result and discussion

2.1. Chemistry

Compounds **3a**-**3g** and **5a**-**5i** were synthesized by the classical method of imine formation involving condensation between aromatic amine with a variety of aromatic aldehydes in ethanol under reflux condition (Scheme 1). Imines were obtained as sole product. Structures of all synthesized compounds were characterized by comparison with ^{1}H and ^{13}C nuclear magnetic resonance (NMR) spectroscopy data.

2.2. Inhibition of Aβ_{1-42} self-induced aggregation

The ability of synthesized compounds to inhibit A$\beta_{1–42}$ self-induced aggregation was assessed using the Thioflavin T (ThT) fluorescence assay[47] with curcumin as standard. The results were summarized in Table 2. From the results, it could be seen that many compounds exhibited moderate-to-good potencies (34.4 to 86.1 % at 20 μM, up to IC_{50}: 1.5 μM) compared to that of curcumin (55.7 % at 20 μM, IC_{50}: 18.9 μM). Noticeably, the optimal Aβ_{1-42} aggregation inhibition potency (IC_{50}: 1.5 μM) was provided by compound **5f** that features R_2 = as dimethylamino group at the position 4 of ring B. Replacement of the position 4 of dimethylamino group on ring B (**5f**) by diethylamino group and methoxy group respectively (**5e** and **5g**) were found to reduce the ability of inhibiting Aβ_{1-42} aggregation. When the R_2 = being dimethylamino group on ring B of compound **5f** was replaced by hydroxy group, compound **5d** exhibited the similar inhibitory activity. The methoxy group at the position 3 (R_1) of ring B (**5b** and **5c**) gave better results of the inhibitive activity than that at the

positions 4 or 5 (R_2 or R_3) of ring B (**5e** and **5i**). From the inhibition values of compounds (**3a** vs. **5a**, **3c** vs. **5b** and **3e** vs. **5i**), it appeared that two substituted groups at positions 1 and 4 of ring A (compared to two substituted groups at 1, 3-positions of ring A) seemed to be beneficial to Aβ self-induced aggregation inhibitory activity. According to the inhibition values of the compounds **3a**-**3g**, the substituted groups of hydroxyl, methoxy and pyridine were favorable for inhibition activity. Compounds **3a**, **3b**, **3d**, **3f** and **3g** (IC_{50} = 17.4, 15.2, 7.8, 15.3 and 6.4 μM) showed highly inhibition activity, which was stronger than that of the reference compound curcumin (IC_{50} = 18.9 μM).

*2.3. Docking study of compound **3d** with A$\beta_{1\text{-}42}$*

To further study the interaction mode of compound **3d** for Aβ, molecular docking study was performed using software package MOE 2008.10. The X-ray crystal structure of the protein A$\beta_{1\text{-}42}$ structure (PDB code 1IYT)[48] used in the docking study was obtained from the Protein Data Bank. As shown in Fig. 2, ring A of compound **3d** interacted with the Tyr10 *via* aromatic π-π stacking interaction with the distance centroid of 4.09 Å. A hydrogen bond interaction was found between ring B of compound **3d** and Asp7 residue with the distance of 2.03 Å. These results indicated that the hydrogen bond and π-π interactions played important roles in the stability of the **3d**/A$\beta_{1\text{-}42}$ complex.

2.4. In vitro antioxidant activity assays

The reduction of the oxidative stress was another crucial aspect in designing agents for AD treatment. The antioxidant activities of our synthetic derivatives were

examined by using the ABTS (2,2'-azino-bis(3-ethylbenzthiazoline-6-sulfonic acid)) radical scavenging method.[49] Their ability to scavenge radicals was shown as IC_{50} and trolox, a water-soluble vitamin E analog, was used as a reference standard. The IC_{50} values of all tested compounds were summarized in Table 2. From the table, it could be seen that compounds **3b**, **3d**, **3f**, **5b, 5c, 5d** and **5i** had much better scavenging activities than trolox, while compounds **3a**, **5f**, **5g** and **5h** had no or little radical scavenging activities compared to trolox. These results indicated that -OH and $-OCH_3$ groups were critical in determination of scavenging activity and Cl, $-N(CH_3)_2$ and $-N(CH_2CH_3)_2$ groups were not favorable for antioxidant activities. Compounds with -OH or $-OCH_3$ groups at positions 3 or 5 (R_1 or R_3) of the ring B, exhibited the most potent scavenging activities (**3b**, **3c, 3d, 3e, 5b, 5c and 5i**), which suggested that the positions of -OH or $–OCH_3$ groups seem to be beneficial to their activities. Furthermore, the simultaneous presence of two *ortho*-positions of OH group and N atom on the same ring seem to play an important role in the antioxidant activities (**3f** and **5c**). Besides, from the inhibition values of compounds (**5a** vs. **3a**, **5b** vs. **3c** and **5i** vs. **3e**), it appeared that two substituted groups at 1, 3-positions of ring A (compared to two substituted groups at 1, 4-positions of ring A) seemed to be beneficial to scavenging activity. Among the target compounds, compounds **3b**, **3d**, **3f** and **5c** (IC_{50} = 3.47, 1.82, 2.94 and 6.14 μM) showed the most potent scavenging activity, which was stronger than that of the reference compound trolox (IC_{50} = 26.14 μM).

2.5. Radical-scavenging activity

Some selected compounds tested for their antioxidant activities (ABTS) were also

tested for their DPPH (diphenyl-1-picrylhydrazyl) radical scavenging activities. DPPH radicals was used in preliminary screening of compounds capable of scavenging ROS, since these nitrogen radicals were much more stable and easier to handle than oxygen free radicals.[50] For comparison purpose, resveratrol was used as reference compound. The IC_{50} values of these selected compounds were summarized in Table 3. Compounds **3b**, **3d**, **3f** and **5c** (IC_{50} = 24.3, 15.4, 29.1 and 45.7 μM) showed good potent scavenging activities, which was 4.3, 6.8, 3.6 and 2.3 times stronger than that of the reference compound resveratrol (IC_{50} = 104.3 μM). These results indicated that the simultaneous presence of two *ortho*- or *para*-positions of OH or OCH_3 group and nitrogen atom on the same ring seem to play an important role in the antioxidant activities.

2.6. Inhibition of MAOs in Vitro

To further study the multipotent biological profile of these selected compounds, the inhibitory activity against the A and B isoforms of *h*MAO was determined. Ladostigil, which was a multifunctional agent with MAO-B inhibition activity approved to carry out phase II clinical trial by FDA, was used as a reference standard. As shown in Table 3, these selected compounds were effective in inhibiting MAO-B in the micromolar range. Among these target compounds, compound **3d** (IC_{50} = 6.4 μM) showed the most potent MAO-B inhibitory activity, which was about 5.7-fold more potent than ladostigil (IC_{50} = 36.2 μM).

2.7. Metal chelating effect

The chelating effect of all compounds for metals such as Cu^{2+} and Fe^{2+} in methanol

was studied by UV–vis spectrometry with wavelength ranging from 200 to 500 nm.[52,53] In Fig. 3a, UV–vis spectra of compound **3d** at increasing Cu^{2+} concentrations were shown as an example. The original spectrum of compound **3d** (without adding metal iron) is the red line. The increase in absorbance (at about 440 nm peak in fig. 3b) and the decrease in absorbance (at about 375 nm peak in fig. 3b), which could be better estimated by an inspection of the differential spectra (Fig. 3b), indicated that there was an interaction between Cu^{2+} and compound **3d**. Similar behavior was also observed when using Fe^{2+}. These observations indicated that our compounds could effectively chelate Cu^{2+} and Fe^{2+}, and thereby could serve as metal chelators in treating AD. The ratio of ligand/metal ion in the complex was investigated by mixing the fixed amount metal ion with increasing ligand; it was possible to observe that the maximum intensity of difference spectra was reach at about 1:1.6 ratio (ratio of ligand/metal ion), which was taken as an indication of the stoichiometry of the complex.

To Further describe the stoichiometry of the complex **3d**−Cu(II), the molar ratio method was used by preparing solutions of compound **3d** with increasing amounts of $CuCl_2$. We used the UV spectra to obtain the absorbance of the complex of $CuSO_4$ and **3d** at different concentrations at 450 nm. According to the following Fig. 4, the absorbance linearly increased at first. When the mole fraction of Cu(II) to **3d** was more than 1.6, the absorbance tended to be stable. Therefore, two straight lines were drawn with the intersection point at a mole fraction of 1.6, revealing a 1:1.6 stoichiometry for complex **3d**−Cu(II).

2.8. Inhibition of Cu^{2+}-induced Aβ_{1-42} aggregation

To further investigate the ability of these selected compounds to inhibit Cu^{2+}-induced Aβ_{1-42} aggregation, we studied compounds **3d**, **3f** and **5c** by a ThT-binding assay.[54] Resveratrol and clioquinol were used as reference compounds. It could be seen from Fig. 5, the fluorescence of Aβ_{1-42} treated with Cu^{2+} is 141.9% that of Aβ_{1-42} alone, which indicates that Cu^{2+} accelerates Aβ_{1-42} aggregation. By contrast, the fluorescence of Aβ_{1-42} treated with Cu^{2+} and the tested compounds decreased dramatically (**3d**, 72.8% inhibition of Cu^{2+}-induced Aβ_{1-42} aggregation; **3f**, 70.5% inhibition; **5c**, 84.1% inhibition; CQ, 61.4% inhibition; Res, 58.3% inhibition). These results suggested that our compounds could inhibit Cu^{2+}-induced Aβ_{1-42} aggregation effectively by chelating Cu^{2+}.

*2.9. Control of Cu^{2+}-Aβ_{1-42} H_2O_2 production by compounds **3d** and **5c***

Binding of redox active metal ions such as Cu^{2+} to Aβ species was known to be involved in generation of ROS such as H_2O_2 and subsequent facilitation of Aβ aggregation and neurotoxicity. The effect of compounds **3d** and **5c** on H_2O_2 production by Cu^{2+}-Aβ_{1-42} species was examined using the HRP/Amplex Red assay.[55] Under reducing conditions, the Cu^{2+}-Aβ_{1-42} reacted with O_2 to generate H_2O_2. Addition of compounds **3d** or **5c** to such a solution reduced the production of H_2O_2 by about 83% and 78% respectively for the Cu^{2+}-Aβ_{1-42} species. By comparison, the strong chelator ethylenediaminetetraacetic acid (EDTA) showed an even more pronounced effect, almost complete eliminating (>90%), and clioquinol (CQ) showed the reducing effect by about 72%. These results showed that compounds **3d** and **5c**

were able to chelate metal ions as well as regulated ROS production, which showed promise for their further applications (Fig. 6).

2.10. Cytotoxicity of synthetic compounds in PC12 cells and neuroprotective effect on H_2O_2-induced oxidative cell damage in PC12 cells

To gain insight into the therapeutic potential of these derivatives, cell viability and neuroprotective capacity against oxidative stress were determined by colorimetric MTT [3-(4, 5-dimethyl-2-thiazolyl)-2, 5-diphenyl-2*H*-tetrazolium bromide] assay[56] in the neuroblastoma cells (PC12). Compounds **3b**, **3d**, **3f**, **5c** and **5f** were selected as representative compounds of different types. The cells were incubated with varying concentrations (1-50 μM) of the test compounds for 24 h and under the conditions these compounds were nontoxic to PC12 cells at any of the concentrations tested (Fig. 7).

The MTT assay[56] was performed to evaluate the effect of these selected compounds on H_2O_2-induced PC12 cell toxicity. Trolox was used as the reference compound. In this assay, addition of 150 μM H_2O_2 to the growth medium reduced cell viability to 70.5% compared to control. The tested compounds were added to the media at different concentrations immediately prior to the H_2O_2 insult. Phase-contrast micrographs showed H_2O_2-induced neurotoxicity and neuroprotection in the rat pheochromocytoma cell line PC12 for the tested compounds (Fig. 8). As can be seen in Fig. 9, all of the compounds exhibited significant neuroprotective against H_2O_2 induced PC12 cell toxicity at concentrations ranging from 1 to 10 μM. Compound **3d** had showed the highest protective capability the same as trolox at the concentration of

3 μM. Compounds **3f** and **5c** showed good protective capabilities similar to trolox at the concentration of 5 μM. This result indicated that the neuroprotective action of our synthesized compounds might come from radical scavenging action.

2.11. Cell viability and neuroprotection against $A\beta_{1\text{-}42}$-induced toxicity

To investigate the effect of the selected compounds on cell viability, the MTT assay was conducted on SH-SY5Y neuroblastoma cells. The colorimetric MTT [3-(4,5-dimethyl-2-thiazolyl)-2,5-diphenyl-2*H*-tetrazolium bromide] assay[57] was performed to examine the potential cytotoxic effects of compounds **3b**, **3d**, **3f**, **5c** and **5f**. As showed in Fig. 10, compounds **3b**, **3d**, **3f**, **5c** and **5f** did not show significant effect on cell viability at 1–50 μM after incubation for 24 h. This suggested that compounds **3b**, **3d**, **3f**, **5c** and **5f** were nontoxicity to SH-SY5Y cells.

The neuroprotective activity of compounds **3d**, **3f** and **5c** against $A\beta_{1\text{-}42}$-induced cytotoxicity in SH-SY5Y neuroblastoma cells was investigated, since this peptide was the most amyloidogenic isoform of $A\beta_{1\text{-}42}$.[57] Melatonin was used as the reference compound. Treatment of SH-SY5Y cells for 24 h with 30 μM $A\beta_{1\text{-}42}$ caused cell viability to 64.8% compared to control. As can be seed in Fig. 11, all of the selected compounds exhibited neuroprotective effects at concentrations ranging from 1 to 10 μM, with compound **3d** showing the highest protective capability. Compound **3d** showed a significant effect at the dose of 3μM, while compounds **3f** and **5c** revealed a moderate effect at the dose of 5 μM, when compared with the 30 μM $A\beta_{1\text{-}42}$ only treated control. Thus, the protective action against the $A\beta_{1\text{-}42}$ peptide of our synthetic compounds might be enhanced by the anti-$A\beta$ aggregation action.

2.12. In vitro blood–brain barrier permeation assay

In the central nervous system (CNS) drug development, it is important that the compounds are able to cross the blood-brain barrier (BBB). So BBB permeability properties of CNS drug candidates should be determined as early as possible in the drug discovery process. To evaluate the potential for these compounds to cross the blood-brain barrier (BBB), we used a parallel artificial membrane permeation assay for BBB (PAMPA-BBB), which was described by Di *et* al.[58] The *in vitro* permeabilities (P_e) of our compounds and 9 commercial drugs through a lipid extract of porcine brain were determined using a mixture of PBS/EtOH (70:30). Assay validation was performed by comparing the experimental permeability with the reported values of these commercial drugs, which gave a good linear correlation, P_e (exptl) = 0.7468P_e (bibl) – 0.2655 (R^2 = 0.9212) (see the Supporting Information, Table S1 and Figure S1). From this equation and taking into account the described limits for BBB permeation, we found that compounds with permeability values above 2.72×10^{-6} cm s^{-1} could penetrate into the CNS by passive diffusion. With the exception of compound **5h**, all compounds showed permeability values over this limit, pointing out that these compounds could cross the BBB (Table 1). From these results, we could conclude that polar groups such as OH, OCH_3 and $N(CH_3)_2$ in this type structure were favorable for BBB permeation.

3. Conclusion

In conclusion, most synthesized compounds exhibited multifunctional activities as potential anti-AD drugs, which included significant ability to inhibit self-induced

A$\beta_{1\text{-}42}$ aggregation and to act as antioxidants and biometal chelators. Among the synthesized compounds, compound **3d** with two *para*-positions of OH groups showed a balanced multifunctional profile covering anti-β-amyloid (Aβ) aggregation, antioxidant, monoamine oxidase B (MAO-B) inhibition, metal chelation, and neuroprotective properties at low micromolar concentrations. Compound **3d** gave the high inhibitory potency toward self-induced A$\beta_{1\text{-}42}$ aggregation (IC_{50} = 7.8 μM) and Cu^{2+}-induced A$\beta_{1\text{-}42}$ aggregation. Meanwhile, this compound was also an excellent antioxidant [IC_{50} (ABTS) = 1.82 μM; IC_{50} (DPPH) = 15.4 μM] and MAO-B inhibitor (IC_{50} = 6.4 μM). In addition, it showed excellent metal chelating property and was capable of decrease reactive oxygen species (ROS) induced by Cu^{2+}-A$\beta_{1\text{-}42}$. Furthermore, compound **3d** showed nontoxic to neuroblastoma cells (PC12 cells and SH-SY5Y neuroblastoma cells) at any of the concentrations tested and a neuroprotective effect against neuronal death induced by oxidative stress and β-amyloid (A$\beta_{1\text{-}42}$), and could cross the blood–brain barrier (BBB). Such multifunctional properties highlighted compound **3d** as a new multifunctional drug candidate for further studies in the treatment of AD.

4. Experimental section

4.1. Chemistry

All chemicals (reagent grade) used were purchased from Sinopharm Chemical Reagent Co., Ltd. (China). Reaction progress was monitored using analytical thin layer chromatography (TLC) on precoated silica gel GF_{254} (Qingdao Haiyang Chemical Plant, Qingdao, China) plates and the spots were detected under UV light

(254 nm). Melting point was measured on an XT-4 micromelting point instrument and uncorrected. IR (KBr-disc) spectra were recorded by Bruker Tensor 27 spectrometer. ^{1}H NMR and ^{13}C NMR spectra were measured on a Bruker ACF-500 spectrometer at 25°C and referenced to TMS. Chemical shifts were reported in ppm (δ) using the residual solvent line as internal standard. Splitting patterns were designed as s, singlet; d, doublet; t, triplet; m, multiplet. Mass spectra were obtained on a MS Agilent 1100 Series LC/MSD Trap mass spectrometer (ESI-MS).

*4.2. General procedures for the preparation of compounds **3a-3g** and **5a-5i***

Two equivalents of the respective salicylaldehyde derivatives (7.0 mmol) in ethanol (20mL) were added dropwise to a solution of one equivalent of 1, 3-phenylenediamine derivatives or 1, 4-phenylenediamine derivatives in ethanol (10 mL). The mixture was stirred under reflux for 1-5 h and then allowed to cool down to room temperature. The product was collected, washed with ethanol and dried (P_2O_5).

4.3.1. 2,2'-((1,4-phenylenebis(azanylylidene))bis(methanylylidene))diphenol (**3a,** CAS: 5344-68-3).

Yield 72%, red solid, m.p. 229-230 ℃; IR (KBr) *v* 2987.97, 1610.26, 1569.63, 1494.99, 1370.56, 1282.46, 1189.12, 1160.90, 1148.81, 1065.80, 906.61, 828.42, 750.33, 618.02, 561.83, 524.42, 484.07, 420.69 cm^{-1}. ^{1}H NMR (500 MHz, DMSO) δ 13.07 (s, 2H), 9.05 (s, 2H), 7.70 (dd, J = 7.7, 1.6 Hz, 2H), 7.57 (s, 4H), 7.47 – 7.44 (m, 2H), 7.04 – 6.99 (m, 4H). ^{13}C NMR (125 MHz, DMSO) δ 163.57, 160.80, 147.19, 133.77, 133.02, 122.99, 119.87, 119.64, 117.09. ESI-MS *m/z*: 317.02 $[M+H]^+$. HRMS (ESI) *m/z* = 315.1139 calcd. for $C_{20}H_{15}N_2O_2$ $[M-H]^-$, found: 315.1140.

4.3.2. 3,3'-((1,4-phenylenebis(azanylylidene))bis(methanylylidene))bis(ben zene-1,2-diol) (**3b,** CAS: 303216-29-7)

Yield 77%, brown solid, m.p. > 250 °C; IR (KBr) *v* 3328.92, 1618.57, 1511.20, 1460.67, 1365.45, 1221.47, 1075.08, 1029.05, 836.17, 731.63, 556.29cm^{-1}. ^{1}H NMR (500 MHz, DMSO) *δ* 13.17 (s, 2H), 9.21 (s, 2H), 9.01 (s, 2H), 7.56 (s, 4H), 7.14 (dd, *J* = 7.8, 1.3 Hz, 2H), 6.98 (dd, *J* = 7.8, 1.4 Hz, 2H), 6.83 (t, *J* = 7.8 Hz, 2H). ^{13}C NMR (125 MHz, DMSO) *δ* 163.47, 149.33, 146.43, 145.60, 122.77, 122.46, 119.42, 119.01, 118.78. ESI-MS *m/z*: 349.03 $[M+H]^+$. HRMS (ESI) *m/z* = 349.1183 calcd. for $C_{20}H_{17}N_2O_4$ $[M+H]^+$, found: 349.1184.

4.3.3 6,6'-((1,4-phenylenebis(azanylylidene))bis(methanylylidene))bis(2-m ethoxy phenol) (**3c**, CAS: 19264-44-9)

Yield 82%, red solid, m.p. 239 °C; IR (KBr) *v* 3451.35, 2939.99, 2835.03, 1606.69, 1468.47, 1362.73, 1274.14, 1255.08, 1200.73, 1167.99, 1093.71, 1077.78, 972.13, 848.89, 836.43, 777.76, 734.10, 721.24, 594.28 cm^{-1}. ^{1}H NMR (500 MHz, DMSO) *δ* 13.21 (s, 2H), 9.05 (s, 2H), 7.57 (s, 4H), 7.42 – 6.95 (m, 6H), 3.86 (s, 6H). ^{13}C NMR (125 MHz, DMSO) *δ* 163.71, 151.11, 148.44, 147.03, 124.43, 123.00, 119.83, 119.14, 116.30, 56.51. ESI-MS *m/z*: 377.08 $[M+H]^+$. HRMS (ESI) *m/z* = 377.1496 calcd. for $C_{22}H_{21}N_2O_4$ $[M+H]^+$, found: 377.1494.

4.3.4 2,2'-((1,4-phenylenebis(azanylylidene))bis(methanylylidene))bis(ben zene-1,4-diol) (**3d**, CAS: 300404-48-2)

Yield 55%, dark red solid, m.p. > 250 °C; IR (KBr) *v* 3267.94, 1581.31, 1467.90, 1411.71, 1314.89, 1276.21, 1242.40, 1220.71, 1204.20, 1157.76, 1117.70, 956.24,

869.47, 838.85, 817.65, 788.59, 757.92, 650.37, 532.64 cm^{-1}. ^1H NMR (500 MHz, DMSO) δ 12.25 (s, 2H), 9.10 (s, 2H), 8.93 (s, 2H), 7.52 (s, 4H), 7.08 (d, J = 2.9 Hz, 2H), 6.90 (dd, J = 8.8, 2.9 Hz, 2H), 6.83 (d, J = 8.8 Hz, 2H). ^{13}C NMR (125 MHz, DMSO) δ 162.65, 153.12, 149.63, 146.90, 122.44, 121.17, 119.34, 117.16, 116.88. ESI-MS *m/z*: 349.02 $[M+H]^+$. HRMS (ESI) *m/z* = 349.1183 calcd. for $C_{20}H_{17}N_2O_4$ $[M+H]^+$, found: 349.1180.

4.3.5. 2,2'-((1,4-phenylenebis(azanylylidene))bis(methanylylidene))bis(4-m ethoxy phenol) (**3e**, CAS: 635750-54-8)

Yield 88%, yellow solid, m.p. 240 °C; IR (KBr) *v* 2937.04, 2831.46, 1576.97, 1497.22, 1456.51, 1396.26, 1363.75, 1273.87, 1216.70, 1181.22, 1161.74, 1125.05, 1050.64, 968.76, 943.07, 872.55, 833.66, 796.06, 736.94, 651.11, 529.14 cm^{-1}. ^1H NMR (500 MHz, DMSO) δ 12.41 (s, 2H), 9.02 (s, 2H), 7.54 (s, 4H), 7.29 (d, J = 3.1 Hz, 2H), 7.08 (dd, J = 8.9, 3.1 Hz, 2H), 6.94 (d, J = 8.9 Hz, 2H), 3.79 (s, 6H). ^{13}C NMR (125 MHz, DMSO) δ 163.08, 154.87, 152.45, 147.45, 122.99, 121.09, 119.80, 117.98, 115.67, 56.51. ESI-MS *m/z*: 377.05 $[M+H]^+$. HRMS (ESI) *m/z* = 377.1496 calcd. for $C_{22}H_{21}N_2O_4$ $[M+H]^+$, found: 377.1495.

4.3.6. 2,2'-((1,4-phenylenebis(methanylylidene))bis(azanylylidene))diphenol (**3f**, CAS: 13060-68-9)

Yield 55%, yellow solid, m.p. 234-235 °C; IR (KBr) *v* 3454.32, 3366.86, 1622.90, 1484.43, 1382.18, 1288.27, 1242.06, 1150.81, 1031.72, 969.10, 924.16, 843.61, 828.05, 776.97, 732.43, 597.17, 563.17, 517.20, 422.92 cm^{-1}. ^1H NMR (500 MHz, DMSO) δ 9.08 (s, 2H), 8.82 (s, 2H), 8.18 (s, 4H), 7.29 (dd, J = 7.9, 1.5 Hz, 2H), 7.15

– 7.12 (m, 2H), 6.96 – 6.94 (m, 2H), 6.90 – 6.87 (m, 2H). ^{13}C NMR (125 MHz, DMSO) δ 158.95, 151.91, 139.11, 138.11, 129.53, 128.22, 119.98, 119.59, 116.62. ESI-MS *m/z*: 317.04 $[M+H]^+$. HRMS (ESI) *m/z* = 315.1139 calcd. for $C_{20}H_{15}N_2O_2$ $[M-H]^-$, found: 315.1142.

4.3.7. *N*1,*N*4-bis(pyridin-2-ylmethylene)benzene-1,4-diamine (**3g**, CAS: 21756-21-8)

Yield 77%, dark yellow solid, m.p. 166 ℃; IR (KBr) *v* 3451.26, 1618.13, 1580.96, 1493.64, 1461.57, 1433.78, 1353.13, 1196.21, 1141.05, 1086.40, 992.06, 968.23, 844.43, 773.58, 737.04, 613.85, 563.14 cm^{-1}. ^{1}H NMR (500 MHz, DMSO) δ 8.76 (d, *J* = 4.7 Hz, 2H), 8.69 (s, 2H), 8.20 (d, *J* = 7.9 Hz, 2H), 7.99 (td, *J* = 7.6, 1.3 Hz, 2H), 7.56 (dd, *J* = 8.0, 5.4 Hz, 2H), 7.47 (s, 4H). ^{13}C NMR (125 MHz, DMSO) δ 160.86, 154.57, 150.16, 149.49, 137.47, 126.06, 122.77, 121.77. ESI-MS *m/z*: 286.98 $[M+H]^+$. HRMS (ESI) *m/z* = 285.1146 calcd. for $C_{18}H_{14}N_4$ $[M-H]^-$, found: 285.1143.

4.3.8. 2,2'-((1,3-phenylenebis(azanylylidene))bis(methanylylidene))diphenol (**5a**, CAS: 17911-94-3)

Yield 64%, yellow solid, m.p. 119 ℃; IR (KBr) *v* 1566.28, 1496.49, 1460.27, 1409.28, 1360.75, 1282.32, 1195.29, 1152.04, 1135.42, 1031.49, 976.11, 951.46, 897.96, 886.75, 818.91, 801.49, 754.64, 688.49, 562.20, 484.96 cm^{-1}. ^{1}H NMR (500 MHz, DMSO) δ 13.02 (s, 2H), 9.07 (s, 2H), 7.70 (d, *J* = 7.6 Hz, 2H), 7.56 (d, *J* = 7.9 Hz, 1H), 7.54 (d, *J* = 1.8 Hz, 1H), 7.48 – 7.43 (m, 2H), 7.38 (dd, *J* = 7.9, 1.9 Hz, 2H), 7.02 (t, *J* = 7.9 Hz, 4H). ^{13}C NMR (125 MHz, DMSO) δ 164.60, 160.83, 149.83, 133.94, 133.11, 130.84, 120.62, 119.80, 119.69, 117.14, 114.32. ESI-MS *m/z*: 317.02

$[M+H]^+$. HRMS (ESI) *m/z* = 315.1139 calcd. for $C_{20}H_{15}N_2O_2$ $[M-H]^-$, found: 315.1141.

4.3.9. 6,6'-((1,3-phenylenebis(azanylylidene))bis(methanylylidene))bis(2-m ethoxy phenol) (**5b**, CAS: 100435-31-2)

Yield 83%, dark yellow solid, m.p. 144 °C; IR (KBr) ν 3741.59, 2310.10, 1578.65, 1465.41, 1252.74, 1172.69, 1136.68, 1078.11, 973.02, 885.00, 836.66, 812.92, 791.43, 727.46, 690.77 cm^{-1}. ^1H NMR (500 MHz, DMSO) δ 13.15 (s, 2H), 9.06 (s, 2H), 7.57 – 7.54 (m, 2H), 7.37 (dd, *J* = 7.9, 1.8 Hz, 2H), 7.28 (d, *J* = 7.8 Hz, 2H), 7.16 (d, *J* = 8.0 Hz, 2H), 6.95 (t, *J* = 7.9 Hz, 2H), 3.85 (s, 6H). ^{13}C NMR (125 MHz, DMSO) δ 164.23, 150.60, 149.08, 147.91, 130.32, 123.94, 120.16, 119.18, 118.62, 115.76, 113.64, 55.88. ESI-MS *m/z*: 377.06 $[M+H]^+$. HRMS (ESI) *m/z* = 377.1496 calcd. for $C_{22}H_{21}N_2O_4$ $[M+H]^+$, found: 377.1498.

4.3.10. 6,6'-((4-hydroxy-1,3-phenylene)bis(azanylylidene))bis(methanylyli dene))bis (2-methoxyphenol) (**5c**)

Yield 58%, yellow solid, m.p. 191 °C; IR (KBr) *v* 2968.21, 2378.33, 2349.11, 2314.62, 1619.02, 1506.68, 1463.46, 1402.87, 1366.63, 1253.04, 1208.39, 1076.49, 975.71, 825.88, 781.13, 739.34, 574.60, 430.38 cm^{-1}. ^1H NMR (500 MHz, $CDCl_3$) δ 10.10 (s, 1H), 9.09 (s, 1H), 9.00 (s, 1H), 7.61 (d, *J* = 2.5 Hz, 1H), 7.28 (dd, *J* = 8.6, 2.5 Hz, 1H), 7.23 – 7.20 (m, 2H), 7.11 (d, *J* = 8.0 Hz, 2H), 7.05 (d, *J* = 8.6 Hz, 1H), 6.90 (dt, *J* = 10.2, 7.9 Hz, 2H), 3.82 (s, 6H). ^{13}C NMR (125 MHz, DMSO) δ 162.39, 161.24, 151.73, 150.53, 150.42, 148.15, 147.87, 139.71, 135.07, 123.85, 123.68, 121.53, 119.28, 119.19, 118.49, 118.07, 116.95, 115.41, 115.28, 112.02, 55.88, 55.85.

ESI-MS *m/z*: 393.06 $[M+H]^+$. HRMS (ESI) *m/z* = 393.1445 calcd. for $C_{22}H_{21}N_2O_4$ $[M+H]^+$, found: 393.1443.

4.3.11. 4,4'-((1,3-phenylenebis(azanylylidene))bis(methanylylidene))bis(be nzene-1,3-diol) (**5d**, CAS: 158116-81-5)

Yield 60%, yellow solid, m.p. > 250°C; IR (KBr) *v* 3057.21, 1596.20, 1505.86, 1466.57, 1343.33, 1312.57, 1241.73, 1191.88, 1111.26, 981.13, 864.19, 789.47, 739.85, 676.47, 607.20, 530.18, 496.03, 421.25 cm^{-1}. ^1H NMR (500 MHz, DMSO) δ 13.50 (s, 2H), 10.30 (s, 2H), 8.90 (s, 2H), 7.50 – 7.46 (m, 3H), 7.39 (s, 1H), 7.25 (dd, *J* = 7.9, 1.9 Hz, 2H), 6.44 (dd, *J* = 8.5, 2.2 Hz, 2H), 6.34 (d, *J* = 2.2 Hz, 2H). ^{13}C NMR (125 MHz, DMSO) δ 163.63, 163.58, 163.14, 149.84, 135.01, 130.71, 119.66, 113.63, 112.57, 108.47, 102.93. ESI-MS *m/z*: 349.02 $[M+H]^+$. HRMS (ESI) *m/z* = 349.1183 calcd. for $C_{20}H_{17}N_2O_4$ $[M+H]^+$, found: 349.1182.

4.3.12. 6,6'-((1,3-phenylenebis(azanylylidene))bis(methanylylidene))bis(3- methoxy phenol) (**5e**)

Yield 75%, dark yellow solid, m.p. 166 °C; IR (KBr) *v* 2969.58, 2310.64, 1623.44, 1588.31, 1512.79, 1462.41, 1440.32, 1405.56, 1340.74, 1287.53, 1234.39, 1205.91, 1170.28, 1134.64, 1116.97, 1030.98, 965.46, 880.26, 834.31, 804.84, 772.82, 686.15, 646.41, 581.72, 524.51, 474.53 cm^{-1}. ^1H NMR (500 MHz, DMSO) δ 13.61 (s, 2H), 8.96 (s, 2H), 7.56 (d, *J* = 8.7 Hz, 2H), 7.50 (t, *J* = 7.9 Hz, 1H), 7.45 (s, 1H), 7.29 (dd, *J* = 7.9, 2.0 Hz, 2H), 6.59 (dd, *J* = 8.6, 2.4 Hz, 2H), 6.53 (d, *J* = 2.4 Hz, 2H), 3.83 (s, 6H). ^{13}C NMR (125 MHz, DMSO) δ 164.33, 163.73, 163.57, 149.57, 134.70, 130.76,

119.91, 113.81, 113.49, 107.40, 101.38, 55.98. ESI-MS *m/z*: 377.02 $[M+H]^+$. HRMS (ESI) *m/z* = 377.1496 calcd. for $C_{22}H_{21}N_2O_4$ $[M+H]^+$, found: 377.1498.

4.3.13. 6,6'-((1,3-phenylenebis(azanylylidene))bis(methanylylidene))bis(3-(d imethyl amino)phenol) (**5f**)

Yield 79%, dark yellow solid, m.p. 208 ℃; IR (KBr) *v* 2902.95, 1631.15, 1578.22, 1523.52, 1444.12, 1410.24, 1358.71, 1269.59, 1217.08, 1129.37, 975.63, 914.83, 874.89, 816.86, 775.71, 683.89, 646.45, 547.88, 469.64 cm^{-1}. ^1H NMR (500 MHz, DMSO) δ 13.61 (s, 2H), 8.82 (s, 2H), 7.44 (t, *J* = 7.9 Hz, 1H), 7.39 (d, *J* = 8.8 Hz, 2H), 7.33 (s, 1H), 7.18 (dd, *J* = 7.9, 1.9 Hz, 2H), 6.39 (dd, *J* = 8.8, 2.4 Hz, 2H), 6.14 (d, *J* = 2.3 Hz, 2H), 3.03 (s, 12H). ^{13}C NMR (125 MHz, DMSO) δ 163.57, 162.61, 154.53, 149.98, 134.47, 130.61, 118.94, 112.98, 109.53, 104.78, 98.11, 56.52. ESI-MS *m/z*:403.14 $[M+H]^+$. HRMS (ESI) *m/z* = 403.2129 calcd. for $C_{24}H_{27}N_4O_2$ $[M+H]^+$, found: 403.2128.

4.3.14. 6,6'-((1,3-phenylenebis(azanylylidene))bis(methanylylidene))bis(3-(d iethyl amino)phenol) (**5g**)

Yield 61%, dark yellow solid, m.p. 152 ℃; IR (KBr) *v* 2969.58, 2930.30, 2311.63, 1631.91, 1573.83, 1517.39, 1476.90, 1424.63, 1376.35, 1350.93, 1303.17, 1240.67, 1220.09, 1193.15, 1158.61, 1129.87, 1077.75, 1013.52, 982.88, 950.15, 893.24, 877.97, 829.77, 785.60, 709.09, 691.21, 655.61, 587.57, 514.72, 470.62, 443.13 cm^{-1}. ^1H NMR (500 MHz, DMSO) δ 13.63 (s, 2H), 8.78 (s, 2H), 7.43 (t, *J* = 7.9 Hz, 1H), 7.36 (d, *J* = 8.9 Hz, 2H), 7.31 (s, 1H), 7.16 (dd, *J* = 7.9, 1.7 Hz, 2H), 6.34 (dd, *J* = 8.8, 2.2 Hz, 2H), 6.10 (d, *J* = 2.0 Hz, 2H), 3.41 (q, *J* = 6.9 Hz, 8H), 1.14 (t, *J* = 7.0 Hz,

12H). ^{13}C NMR (125 MHz, DMSO) δ 163.98, 162.23, 152.18, 150.00, 134.76, 130.60, 118.72, 112.92, 109.13, 104.42, 97.42, 44.42, 13.05. ESI-MS *m/z*: 459.20 $[M+H]^+$. HRMS (ESI) *m/z* = 459.2756 calcd. for $C_{28}H_{35}N_4O_2$ $[M+H]^+$, found: 459.2755.

4.3.15. 2,2'-((1,3-phenylenebis(azanylylidene))bis(methanylylidene))bis(4- chloro phenol) (**5h**, CAS: 346588-04-3)

Yield 70%, yellow solid, m.p. 241 ℃; IR (KBr) *v* 1618.54, 1566.79, 1482.62, 1390.65, 1353.01, 1314.29, 1277.27, 1193.13, 1133.53, 1091.15, 997.35, 954.37, 928.37, 892.18, 823.10, 786.21, 729.57, 695.99, 647.19, 560.25, 494.21cm^{-1}. ^{1}H NMR (500 MHz, DMSO) δ 12.87 (s, 2H), 9.04 (s, 2H), 7.79 (d, *J* = 2.7 Hz, 2H), 7.58 (t, *J* = 7.9 Hz, 1H), 7.51 (t, *J* = 1.9 Hz, 1H), 7.49 (dd, *J* = 8.8, 2.7 Hz, 2H), 7.40 (dd, *J* = 7.9, 2.0 Hz, 2H), 7.05 (d, *J* = 8.8 Hz, 2H). ^{13}C NMR (125 MHz, DMSO) δ 163.04, 159.40, 149.73, 133.42, 131.46, 130.95, 123.15, 121.14, 120.77, 119.20, 114.70. ESI-MS *m/z*: 384.98 $[M+H]^+$. HRMS (ESI) *m/z* = 385.0505 calcd. for $C_{20}H_{14}Cl_2N_2O_2$ $[M+H]^+$, found: 385.0507.

4.3.16. 2,2'-((1,3-phenylenebis(azanylylidene))bis(methanylylidene))bis(4- methoxy phenol) (**5i**, CAS: 346587-99-3)

Yield 67%, yellow solid, m.p. 160 ℃; IR (KBr) *v* 3742.31, 2965.18, 2378.09, 2309.82, 1570.68, 1492.10, 1390.51, 1355.00, 1333.91, 1277.42, 1249.23, 1221.19, 1189.00, 1158.57, 1035.26, 962.15, 879.91, 855.40, 834.53, 811.12, 781.00, 674.19, 582.51, 468.78 cm^{-1}. ^{1}H NMR (500 MHz, DMSO) δ 12.40 (s, 2H), 9.02 (s, 2H), 7.54 (t, *J* = 7.9 Hz, 1H), 7.48 (s, 1H), 7.34 (dd, *J* = 7.9, 1.9 Hz, 2H), 7.28 (d, *J* = 3.1 Hz, 2H), 7.07 (dd, *J* = 8.9, 3.1 Hz, 2H), 6.94 (d, *J* = 8.9 Hz, 2H), 3.78 (s, 6H). ^{13}C NMR

(125 MHz, DMSO) δ 164.05, 154.91, 152.43, 150.07, 130.82, 121.22, 120.54, 119.68, 118.02, 115.69, 114.16, 56.07. ESI-MS *m/z*: 377.06 $[M+H]^+$. HRMS (ESI) *m/z* = 377.1496 calcd. for $C_{22}H_{21}N_2O_4$ $[M+H]^+$, found: 377.1493.

4.4. Inhibition of Aβ_{1-42} self-induced aggregation

Inhibition of Aβ_{1-42} aggregation was measured using a Thioflavin T (ThT)-binding assay.[47] HFIP pretreated Aβ_{1-42} samples (Anaspec Inc.) were resolubilized with a 50 mM phosphate buffer (pH 7.4) to give a 25 μM solution. Each tested compound was firstly prepared in DMSO at a concentration of 10 mM and 1 μL of each was added to the well of black, opaque Corning 96-well plates such that the final solvent concentration was 10%. The final concentration of each compound was 20 μM and was prepared in independent triplicates. The solvent control was also included. Then, 9 μL of 25 μM Aβ_{1-42} sample was added to each well and the samples mixed by gentle trapping. Plates were covered to minimize evaporation and incubated in dark at room temperature for 46–48 h with no agitation. After the incubation period, 200 μL of 5 μM ThT in 50 mM glycine-NaOH buffer (pH 8.0) was added to each well. Fluorescence was measured on a SpectraMax M5 (Molecular Devices, Sunnyvale, CA, USA) multi-mode plate reader with excitation and emission wavelengths at 446 nm and 490 nm, respectively. The fluorescence intensities were compared and the percent inhibition due to the presence of the inhibitor was calculated by the following formula: $100-(IF_i/IF_o\times100)$ where IF_i and IF_o are the fluorescence intensities obtained for Aβ_{1-42} in the presence and in the absence of inhibitor, respectively.

4.5. Docking study

Molecular modeling calculations and docking studies were performed using Molecular Operating Environment (MOE) software version 2008.10 (Chemical Computing Group, Montreal, Canada). The X-ray crystal structure of A$\beta_{1\text{-}42}$ (PDB 1IYT) used in the docking study was obtained from the Protein Data Bank (www.rcsb.org). Heteroatoms and water molecules in the PDB file were removed at the beginning, and all hydrogen atoms were added to the protein. Amber99 force field was assigned to the enzyme and the partial charges were calculated with the same force field. Protonate states of the enzyme at pH 7 were obtained by following the Protonate 3D protocol in which all configurations were set as default. Compound **3d** was drawn in MOE with all hydrogen atoms added. During the docking procedure, pose of compound **3d** was initially generated by Triangle Matcher method, and scored with london dG function. 30 Poses of the compound were dedicated to the next refinement procedure. All poses were fine tune with the force field refinement scheme. The best 10 poses of molecules were retained and scored. After docking, the geometry of resulting complex was studied using the MOE's pose viewer utility.[48]

4.6. In vitro antioxidant activity assays

The radical scavenging activity of the test compounds was measured by the ABTS method.[49] The ABTS was dissolved in water to obtain a 7 mM concentration of ABTS stock solution. ABTS radical cation ($ABTS^+$) was generated by adding 2.45 mM potassium persulfate to the ABTS stock solution and keeping it in the dark at room temperature for 12-16 h. The $ABTS^+$ solution was diluted with ethanol to give an absorbance of 0.70 ± 0.02 at 734 nm. The 10 ml of the test compounds were allowed

to react with 990 ml of $ABTS^+$ solution. The absorbance was taken 15 min after initial mixing. Trolox was used as a standard.

4.7. DPPH free radical-scavenging assay

DPPH was used to assess free radical-scavenging activity.[50] DPPH was one of the few stable and commercially available organic nitrogen radicals and had a UV–vis absorption maximum at 517 nm. Upon reduction, the solution color fades; the reaction progress was conveniently monitored by a spectrophotometer. To test free radical-scavenging effects, compounds **3a**–**3g** and **5a-5i** were adjusted with methanol solution to final concentrations of 0–200 μM. Methanolic DPPH (400 μM) was used in the reaction mixture. Serial dilutions of the test sample (20 μL) were combined with the DPPH (180 μL, 400 μM) solution in a 96-well microtitre plate. MeOH was used as a negative control and resveratrol was used as positive control. The reaction mixtures were incubated for 30 min at 37 °C in the dark and the change in absorbance at 517 nm was measured. Mean values were obtained from triplicate experiments. Inhibition percent was calculated using the equation: DPPH radical-scavenging rate (%) = [1- (*A* - *C*) / *B*] × 100, where A is the absorbance of the sample (DPPH + compounds), B is the absorbance of the DPPH radical-methanol solution, and C is the absorbance of the sample (compounds) alone. Percent inhibition was plotted against concentration, and the equation for the line was used to obtain the IC_{50} value. The IC_{50} values of samples were compared against the standard, resveratrol, and the lower the IC_{50} of synthesized compounds, the better it was as an antioxidant.

4.8. Inhibition of MAO Activity[51]

The potential effects of the test drugs on *h*MAO activity were investigated by measuring their effects on the production of H_2O_2 from *p*-tyramine, using the Amplex Red MAO assay kit (Molecular Probes, Inc.) and recombinant human MAO-A or MAO-B (Sigma-Aldrich) according to published procedures.

4.9. Spectrophotometric measurement of complex with Cu^{2+} and Fe^{2+}

The study of metal chelation was performed in methanol at 298 K using UV–vis spectrophotometer (SHIMADZU UV-2450PC) with wavelength ranging from 200 to 500 nm.[52,53] The difference UV–vis spectra due to complex formation was obtained by numerical subtraction of the spectra of the metal alone and the compound alone (at the same concentration used in the mixture) from the spectra of the mixture. A fixed amount of **3d** (25 μmol/L) was mixed with growing amounts of copper ion (2–75 μmol/L) and tested the difference UV–vis spectra to investigate the ratio of ligand/metal in the complex. A fixed amount of 3d (50 μM) was mixed with growing amounts of copper ion (8-120 μM), and the difference UV-vis spectra were examined to investigate the ratio of ligand/metal in the complex.

4.10. Inhibition of Cu^{2+}-induced $A\beta_{1-42}$ aggregation

For the inhibition of Cu^{2+}-induced $A\beta_{1-42}$ aggregation experiment,[54] the $A\beta$ was diluted in 20 μM HEPES (pH 6.6) with 150 μM NaCl. The mixture of the peptide (10 μL, 25 μM, final concentration) with or without copper (10 μL, 25 μM, final concentration) and the test compound (10 μL, 50 μM, final concentration) was incubated at 37^{o}C for 24 h. The 20 μL of the sample was diluted to a final volume of 200 μL with 50 mM glycine-NaOH buffer (pH 8.0) containing Thioflavin T (5 μM).

The detection method was the same as that of self-induced Aβ_{1-42} aggregation experiment.

4.11. Hydrogen Peroxide Assays

Hydrogen peroxide production was determined using a HRP/Amplex Red assay. A general protocol from Invitrogen's Amplex Red Hydrogen Peroxide/Peroxidase Assay as followed.[55] Reagents were added directed to a 96-well plate in the following order to give a 100 μL final solution: $CuCl_2$ (400 nM), phosphate buffer, Aβ peptide (200 μM), compounds (800 nM, 1% v/v DMSO), sodium ascorbate (10 μM). The reaction was allowed to incubate for 30 min at room temperature. After this incubation, 50 μM of freshly prepared working solution containing 100 nM Amplex Red (Sigma) and 0.2 U/mL HRP (Sigma) in phosphate buffer was added to each well, and the reaction was allowed to incubate for 30 min at room temperature. Fluorescence was measured using a SpectraMax Paradigm plate reader ($\lambda_{ex}/\lambda_{em}$ = 530/590). Error bars represent standard deviations for at least three measurements.

4.12. Culture of the rat pheochromocytoma PC12 cells[56]

The rat pheochromocytoma PC12 cells were routinely grown at 37°C in a humidified incubator with 5% CO_2 in Dulbecco's modified Eagle's medium (DMEM) supplemented with 10% bovine calf serum, 100 units/mL penicillin, and 100 units/mL of streptomycin. Cells were subcultured in 96-well plates at a seeding density of 1×10^4 cells/well and allowed to adhere and grow. When cells reached the required confluence, they were placed into serum-free medium and treated with compounds **3b**, **3d**, **3f**, **5c** and **5f**. Twenty-four hours later the survival of cells was determined by

MTT assay. The absorbance of each well was measured using a microculture plate reader with a test wavelength of 570 nm and a reference wavelength of 630 nm. Results are expressed as the mean ± SD of three independent experiments.

4.13. Neuroprotection against oxidative stress[56]

To evaluate the protective effects of compounds against hydrogen peroxide induced neurotoxicity, the PC12 cells were seeded in 96-well plates at a density of 2×10^4 per well, incubated for 12 h and subsequently the medium was changed with serum-free DMEM containing 150 μM H_2O_2 and different concentrations (1, 3, 5 and 10 μM) of these selected compounds **3d**, **3f** and **5c**. Cell viability was measured by using the MTT assay after treatment of 150 μM hydrogen peroxide for 24 h.

4.14. Cell culture and MTT assay for cell viability[57]

SH-SY5Y cells, at passages between 3 and 16 after de-freezing, were maintained in a Dulbecco's modified Eagle's medium (DMEM) containing 15 non-essential amino-acids (NEAAs) and supplemented with 10% fetal calf serum (FCS), 1 mM glutamine, 50 units/mL penicillin and 50 μg/mL streptomycin. Cultures were seeded into flasks containing supplemented medium and maintained at 37^{o}C in 5% CO_2/humidified air. Stock cultures were passaged 1:4 twice weekly. Cells were subcultured in 96-well plates at a seeding density of 1×10^5 cells/well and allowed to adhere and grow. When cells reached the required confluence, they were placed into serum-free medium and treated with compounds **3b, 3d**, **3f, 5c** and **5f**. Twenty-four hours later the survival of cells was determined by MTT assay. Briefly, after incubation with 20 μL of MTT at 37°C for 4 h, living cells containing MTT formazan

crystals were solubilized in 200 μL DMSO. The absorbance of each well was measured using a microculture plate reader with a test wavelength of 570 nm and a reference wavelength of 630 nm. Results are expressed as the mean ± SD of three independent experiments.

4.15. Neuroprotection against $A\beta_{1-42}$-induced toxicity[57]

SH-SY5Y cells were seeded at 1×10^5 cells/well in 96-well plates. After 24 h, the medium was removed and replaced with the tested compounds **3d**, **3f** and **5c** (1, 3, 5, 10 μM) at 37°C and incubated for another 24 h. Melatonin was used as the control with concentrations of 10 nM. Then, they were co-incubated for another 24h period with the compound in the presence of $A\beta_{1-42}$ 30 μM. Results are expressed as percent viability compared to untreated cells.

4.16. In vitro blood–brain barrier permeation assay

Brain penetration of compounds was evaluated using a parallel artificial membrane permeation assay (PAMPA) in a similar manner as described by Di et al.[58] Commercial drugs were purchased from Sigma and Alfa Aesar. The porcine brain lipid (PBL) was obtained from Avanti Polar Lipids. The donor microplate (PVDF membrane, pore size 0.45 mm) and the acceptor microplate were both from Millipore. The 96-well UV plate (COSTAR$^{@}$) was from Corning Incorporated. The acceptor 96-well microplate was filled with 300 μL of PBS/EtOH (7:3), and the filter membrane was impregnated with 4 μL of PBL in dodecane (20 mg/mL). Compounds were dissolved in DMSO at 5 mg/mL and diluted 50-fold in PBS/EtOH (7:3) to achieve a concentration of 100 mg/mL, 200 μL of which was added to the donor wells.

The acceptor filter plate was carefully placed on the donor plate to form a sandwich, which was left undisturbed for 16 h at 25℃. After incubation, the donor plate was carefully removed and the concentration of compound in the acceptor wells was determined using a UV plate reader (Flexsta-tion@ 3). Every sample was analyzed at five wavelengths, in four wells, in at least three independent runs, and the results are given as the mean ± standard deviation. In each experiment, 9 quality control standards of known BBB permeability were included to validate the analysis set.

Acknowledgements

This research work was financially supported by Innovative Research Team in University (IRT1193), A Project Funded by the Priority Academic Program Development of Jiangsu Higher Education Institutions (PAPD), Project of Graduate Education Innovation of Jiangsu Province (No. CXZZ13_0320).

References

1 M. Goedert and M.G. Spillantini, *Science*, 2006, **314**, 777-781.

2 W. Thies and L. Bleiler, *Alzheimers Dement.*, 2013, **9**, 208−245.

3 http://www.alz.co.uk/research/files/WorldAlzheimerReport. World Alzheimer Report. 2009. Alzheimer's disease international.

4 E. Scarpini, P. Scheltens and H. Feldman, *Lancet Neurol.*, 2003, **2**, 539-547.

5 M. Chen, Q. Liu, A. Liu, M. Tan, Z. Xie, A. Uri, Z. Chen, G. Huang, Y. Sun, H. Ge, P. Liu, M. Li, X. Li, S. Wen and R. Pi, *RSC Adv.*, 2014, **4**, 37266.

6 A. Cavalli, M.L. Bolognesi, A. Minarini, M. Rosini, V. Tumiatti, M. Recanatini and C. Melchiorre, *J. Med. Chem.*, 2008, **51**, 347-372.

7 B. Sommer, *Curr. Opin. Pharmacol.*, 2002, **2**, 87-92.

8 J. Hardy and D.J. Selkoe, *Science*, 2002, **297**, 353-356.

9 D.J. Selkoe, *Nature.*, 1999, **399**, A23-A31.

10 G. Pepeu and M.G. Giovannini, *Curr. Alzheimer Res.*, 2009, **6**, 86−96.

11 A.I. Bush, *J. Alzheimers Dis.*, 2008, **15**, 223−240.

12 A.S. Pithadia and M.H. Lim, *Curr. Opin. Chem. Biol.*, 2012, **16**, 67–73.

13 S. Boopathi and P. Kolandaivel, *RSC Adv.*, 2014, **4**, 38951.

14 S.C. Drew and K.J. Barnham, *Acc. Chem. Res.*, 2011, **44**, 1146–1155.

15 L.E. Scott and C. Orvig, *Chem. Rev.*, 2009, **109**, 4885–4910.

16 M.G. Savelieff, S. Lee, Y. Liu and M.H. Lim, *ACS Chem. Biol.*, 2013, **8**, 856–865.

17 C. Hureau, *Coord. Chem. Rev.*, 2012, **256**, 2164–2174.

18 C. Hureau and P. Dorlet, *Coord. Chem. Rev.*, 2012, **256**, 2175–2187.

19 J.L. Pierre and M. Fontecave, *Biometals*, 1999, **12**, 195-199.

20 M.I. Fernández-Bachiller, C. Pérez, N.E. Campillo, J.A. Páez, G.C. González-Muñoz, P. Usán, E. García-Palomero, M.G. López, M. Villarroya, A.G. García, A. Martínez and M. I. Rodríguez-Franco, *ChemMedChem*, 2009, **4**, 828-841.

21 D.J. Bonda, X. Wang, G. Perry, A. Nunomura, M. Tabaton, X. Zhu and M.A. Smith, *Neuropharmacology*, 2010, **59**, 290-294.

22 T.M. Bray, *Proc. Soc. Exp. Biol. Med.*, 1999, **222**, 195.

23 K. Beking and A. Vieira, *Public health nutr.*, 2010, **13**, 1403-1409.

24 J.C. Shih, K. Chen and M.J. Ridd, *Annu. Rev. Neurosci.*, 1999, **22**, 197–217.

25 C. Binda, P. Newton-Vinson, F. Hubálek, D.E. Edmondson and A. Mattevi, *Nat. Struct. Biol.*, 2002, **9**, 22–26.

26 F. Hubálek, J. Pohl and D.E. Edmondson, *J. Biol. Chem.*, 2003, **278**, 28612–28618.

27 M.B. Youdim and L. Lavie, *Life Sci.*, 1994, **55**, 2077–2082.

28 N. Hauptmann, J. Grimsby, J.C. Shih and E. Cadenas, *Arch. Biochem. Biophys.*, 1996, **335**, 295–304.

29 L.M. Sayre, G. Perry and M.A. Smith, *Chem. Res. Toxicol.*, 2008, **21**, 172–188.

30 M. Sano, C. Ernesto, R.G. Thomas, M.R. Klauber, K. Schafer, M. Grundman, P. Woodbury, J. Growdon, C.W. Cotman, E. Pfeiffer, L.S. Schneider and L.J. Thal, *N. Engl. J. Med.*, 1997, **336**, 1216−1222.

31 J. Geng, M. Li, L. Wu, J. Ren and X. Qu, *J. Med. Chem.*, 2012, **55**, 9146-9155.

32 M.G. Savelieff, Y. Liu, R.R. Senthamarai, K.J. Korshavn, H.J. Lee, A.

Ramamoorthy and M.H. Lim, *Chem. Commun.*, 2014, **50**, 5301-5303.

33 A. Kochi, T.J. Eckroat, K.D. Green, A.S. Mayhoub, M.H. Lim and S. Garneau-Tsodikova, *Chem. Sci.*, 2013, **4**, 4137-4145.

34 S.S. Xie, X.B. Wang, J.Y. Li, L. Yang and L.Y. Kong, *Eur. J. Med. Chem.*, 2013, **64**, 540-553.

35 S.Y. Li, N. Jiang, S.S. Xie, K.D. Wang, X.B. Wang and L.Y. Kong, *Org. Biomol. Chem.*, 2014, **12**, 801-814.

36 S.Y. Li, X.B. Wang and L.Y. Kong, *Eur. J. Med. Chem.*, 2014, **71**, 36-45.

37 T. Hamaguchi, K. Ono and M. Yamada, *C. N. S. Neurosci. Ther.*, 2010, **16**, 285-297.

38 F. Yang, G.P. Lim, A.N. Begum, O.J. Ubeda, M.R. Simmons, S.S. Ambegaokar, P.P. Chen, R. Kayed, C.G. Glabe, S.A. Frautschy and G.M. Cole, *J. Biol. Chem.*, 2005, **280**, 5892-5901.

39 A.A. Reinke and J.E. Gestwicki, *Chem. Biol. Drug Des.*, 2007, **70**, 206-215.

40 M. Orhan Püsküllü, B. Tekiner and S. Suzen, *Mini Rev. Med. Chem.*, 2013, **13**, 365−372.

41 B.H. Havsteen, *Pharmacol. Ther.*, 2002, **96**, 67−202.

42 C.A. Rice-Evans, N.J. Miller and G. Paganga, *Free Radical Biol. Med.*, 1996, **20**, 933−956.

43 J.S. Choi, J.J. Braymer, R.P. Nanga, A. Ramamoorthy and M.H. Lim, *Proc. Natl. Acad. Sci. U. S. A.*, 2010, **107**, 21990−21995.

44 A.S. Pithadia, A. Kochi, M.T. Soper, M.W. Beck, Y. Liu, S. Lee, A.S. DeToma, B.T. Ruotolo and M.H. Lim, *Inorg. Chem.*, 2012, **51**, 12959−12967.

45 L. Di, E.H. Kerns, K. Fan, O.J. McConnell and G.T. Carter, *Eur. J. Med. Chem.*, 2003, **38**, 223−232.

46 A. Avdeef, S. Bendels, L. Di, B. Faller, M. Kansy, K. Sugano and Y. Yamauchi, *J. Pharm. Sci.*, 2007, **96**, 2893−2909.

47 M. Bartolini, C. Bertucci, M.L. Bolognesi, A. Cavalli, C. Melchiorre and V. Andrisano, *Chembiochem.*, 2007, **8**, 2152-2161.

48 C. Yang, X. Zhu, J. Li and R. Shi, *J. Mol. Model.*, 2010, **16**, 813-821.

49 N.J. Miller and C.A. Rice-Evans, *Free. Radic. Res.*, 1997, **26**, 195-199.

50 J.C. Jung, E. Lim, Y. Lee, J.M. Kang, H. Kim, S. Jang, S. Oh and M. Jung, *Eur. J. Med. Chem.*, 2009, **44**, 3166-3174.

51 F. Chimenti, D. Secci, A. Bolasco, P. Chimenti, B. Bizzarri, A. Granese, S. Carradori, M. Yáñez, F. Orallo, F. Ortuso and S. Alcaro, *J. Med. Chem.*, 2009, **52**, 1935−1942.

52 W. Huang, D. Lv, H. Yu, R. Sheng, S.C. Kim, P. Wu, K. Luo, J. Li and Y. Hu, *Bioorg. Med. Chem.*, 2010, **18**, 5610-5615.

53 R. Joseph, B. Ramanujam, A. Acharya, A. Khutia and C.P. Rao, *J. Org. Chem.*, 2008, **73**, 5745-5758.

54 C. Lu, Y. Guo, J. Yan, Z. Luo, H.B. Luo, M. Yan, L. Huang and X. Li, *J. Med. Chem.*, 2013, **56**, 5843-5859.

55 R.A. Himes, G.Y. Park, G.S. Siluvai, N.J. Blackburn and K.D. Karlin, *Angew. Chem. Int. Ed. Engl.*, 2008, **47**, 9084-9087.

56 M.M. Jin, L. Zhang, H.X. Yu, J. Meng, Z. Sun and R.R. Lu, *Food Chem.*, 2013, **141**, 847–852.

57 G.C. González-Muñoz, M.P. Arce, B. López, C. Pérez, A. Romero, L. del Barrio, M.D. Martín-de-Saavedra, J. Egea, R. León, M. Villarroya, M.G. López, A.G. García, S. Conde and M.I. Rodríguez-Franco, *Eur. J. Med. Chem.*, 2011, **46**, 2224-2235.

58 M.I. Fernández-Bachiller, C. Pérez, L. Monjas, J. Rademann and M.I. Rodríguez-Franco, *J. Med. Chem.*, 2012, **55**, 1303−1317.

Figure and Scheme Captions

Fig. 1. Combination of the main features of curcumin, IMSB, **1** and **2** provides molecules with multifunctionality.

Fig. 2. Docking study of compound **3d** (colored green) with A$\beta_{1\text{-}42}$ (PDB code 1IYT). (a) Cartoon representations of compound **3d** interacting with A$\beta_{1\text{-}42}$. (b) Association of compound **3d** (colored green) and the A$\beta_{1\text{-}42}$ obtained from docking calculations.

The interactions between the ligand and residue Tyr10 and Asp7 are indicated by the green line. (For interpretation of the references to color in this figure legend, the reader is referred to the web version of this article.)

Fig. 3. (a) UV–vis (200–500 nm) absorption spectra of compound **3d** (25 μM) in methanol after addition of ascending amounts of $CuCl_2$ (2–75 μmol/L). The original spectrum of compound **3d** (without adding metal iron) is the red line. (b) The differential spectra due to **3d**-Cu^{2+} complex formation obtained by numerical subtraction from the above spectra of those of Cu^{2+} and **3d** at the corresponding concentrations. The increase in absorbance at about 440 nm peak and the decrease in absorbance at about 375 nm peak.

Fig. 4. Determination of the stoichiometry of complex **3d**-Cu(II) by molar ratio method.

Fig. 5. Inhibition of Cu^{2+}-induced A$\beta_{1\text{-}42}$ aggregation by compounds **3d**, **3f** and **5c** comparing with those of resveratrol (Res) and clioquinol (CQ) ([Aβ = 25 μM, [**3d**] = 50 μM, [**3f**] = 50 μM, [**5c**] = 50 μM, [Res] = 50 μM, [CQ] = 50 μM, [Cu^{2+}] = 25 μM, 37^{o}C, 24h). Values are reported as the mean$\pm$SD of three independent experiments. *p<0.05, **p<0.01.

Fig. 6. Production of H_2O_2 from reactions of Aβ, Cu^{2+}, and compound upon addition of ascorbate, as determined by a HRP/Amplex-Red assay. Lanes: (1) Aβ; (2) Aβ + Cu^{2+}; (3) Aβ + Cu^{2+} + **3d**; (4) Aβ + Cu^{2+} + **5c**; (5) Aβ + Cu^{2+} + CQ; (6) Aβ + Cu^{2+} + EDTA ([Aβ] = 200 nM, [Cu^{2+}] = 400 nM, [chelator] = 800 nM, [ascorbate] = 10 μM, [Amplex Red] = 50 nM, [HRP] = 0.1 U/mL, and $\lambda_{ex/em}$ = 530/590 nm). Values are reported as the mean ± SD of three independent experiments.

Fig. 7. Effects of compounds on cell viability in PC12 cells. The cell viability was determined by the MTT assay after 24h of incubation with various concentrations of

3b, **3d**, **3f**, **5c** and **5f**. The results were expressed as a percentage of control cells. Values are reported as the mean ± SD of three independent experiments.

Fig. 8. Phase-contrast micrographs showing H_2O_2-induced neurotoxicity and neuroprotection of compound **3d** in PC12 cells. (A) Cells without compound treatment showed healthy shapes. (B) Compound **3d** (50 μM) alone did not induce neurotoxicity. (C) H_2O_2 alone (150 μM) induced neurotoxicity. (D) Compound **3d** (3 μM) was given for 24 h with H_2O_2 (150 μM) at 37 °C and co-treatment showed neuroprotection (original magnification, 200).

Fig. 9. Neuroprotection against H_2O_2 toxicity. Compounds **3d**, **3f** and **5c** were tested for neuroprotective activity against H_2O_2 toxicity in PC12 neuroblastoma cell cultures. Trolox (10 μM) was used as the reference compound. Results are expressed as percent viability compared to cells not treated with H_2O_2. Data represent the mean ± SD of three observations. ***$p<0.001$, **$p<0.01$.

Fig. 10. Effects of compounds on cell viability in SH-SY5Y cells. The cell viability was determined by the MTT assay after 24h of incubation with various concentrations of **3b**, **3d**, **3f**, **5c** and **5f**. The results were expressed as a percentage of control cells. Values are reported as the mean ± SD of three independent experiments.

Fig. 11. Neuroprotection against Aβ toxicity. Compounds **3d**, **3f** and **5c** were tested for neuroprotective activity against Aβ toxicity in SH-SY5Y neuroblastoma cell cultures. Melatonin (10 nM) was used as the reference compound. Results are expressed as percent viability compared to cells not treated with Aβ. Data represent the mean ± SD of three observations. ***$p<0.001$, **$p<0.01$.

Scheme 1. Structure scheme of the designed compounds.

Table 1. Properties (MW, clogP, HBA, HBD, PSA, logBB, and P_e)[a] for compounds **3a-3g** and **5a-5i.**

compounds	MW	clogP	HBA	HBD	PSA	log BB	P_e (10^{-6} cm s^{-1})
3a	316	4.026	4	2	65.18	-0.214	6.34
3b	348	3.373	6	4	105.64	-0.912	6.35
3c	376	3.745	6	2	83.64	-0.530	3.19
3d	348	3.233	6	4	105.64	-0.933	5.17
3e	376	4.245	6	2	83.64	-0.454	4.72
3f	316	2.224	4	2	65.18	-0.488	8.12
3g	286	1.074	4	0	49.44	-0.430	4.53
5a	316	4.026	4	2	65.18	-0.214	7.14
5b	376	3.745	6	2	83.64	-0.530	9.31
5c	392	3.078	7	3	103.87	-0.931	4.50
5d	348	3.233	6	4	105.64	-0.933	3.14
5e	376	4.245	6	2	83.64	-0.454	5.67
5f	402	4.667	6	2	71.66	-0.212	7.15
5g	458	6.783	6	2	71.66	0.109	3.53
5h	384	5.660	4	2	65.18	0.035	1.74
5i	376	4.245	6	2	83.64	-0.454	4.58
rules	≤450	≤5.0	≤10	≤5	≤90	≥-1.0	>2.72; <1.23

[a]MW, molecular weight; clogP, calculated logarithm of the octanol−water partition coefficient; HBA, hydrogen bond acceptor atoms; HBD, hydrogen bond donor atoms; PSA, polar surface area; logBB = −0.0148 × PSA + 0.152 × clogP + 0.139 (logBB > 3.0, readily crosses BBB; logBB < −1.0, poorly distributed to the brain); P_e values were determined using the Parallel Artificial Membrane Permeability Assay (PAMPA), P_e (10^{-6} cm s^{-1}) > 2.72 (high BBB permeation), P_e (10^{-6} cm s^{-1}) < 1.23 (low BBB permeation), 1.23 < P_e (10^{-6} cm s^{-1}) < 2.72 (BBB permeation uncertain).

Table 2. Inhibition of self-induced Aβ_{1-42} aggregation and total antioxidant capacity (ABTS) by curcumin, trolox, compounds **3a**-**3g** and **5a**-**5i**.

compounds	Inhibition of Aβ_{1-42} aggregation[a] (%)	IC_{50}[b] (μM)	ABTS assay[c] IC_{50} (μM)
3a	63.1±4.2	17.4±0.7	>200
3b	67.3±3.7	15.2±0.9	3.47
3c	74.1±3.2	n.t.[e]	150.23
3d	72.5±1.4	7.8±1.5	1.82
3e	69.3±2.4	n.t.[e]	114.53
3f	65.2±3.2	15.3±1.7	2.94
3g	78.5±1.7	6.4±1.4	104.41
5a	46.1±4.8	n.t.[e]	47.95
5b	55.6±1.3	n.t.[e]	17.32
5c	77.3±2.4	4.9±0.8	6.14
5d	75.4±1.1	n.t.[e]	23.49
5e	< 20	n.t.[e]	70.18
5f	86.1±2.3	1.5+1.6	>200
5g	< 20	n.t.[e]	>200
5h	< 20	n.t.[e]	>200
5i	34.4±1.3	n.t.[e]	21.73
Curcumin[d]	55.7±2.4	18.9±1.3	n.t.[e]
Trolox[d]	n.t.[e]	n.t.[e]	26.14

[a] The Thioflavin-T fluorescence method was used. Values are expressed as the means ± SD from at least three independent measurements. All of the values were obtained with 20 μM of the tested compounds. [b] The Thioflavin-T fluorescence method was used. Values were expressed as the mean ± SD from at least three independent measurements.

[c] Data were expressed as IC_{50}, the test compound's concentration that inhibits 50% of free radicals (mean ± SD).

[d] Curcumin and trolox were used as positive control.

[e] n.t. = not tested.

Table 3 DPPH scavenging activities and inhibitory activities of human recombinant MAO isoforms of selected compounds.

Compounds	IC_{50} (μM)[a]	IC_{50} (μM)[a]		SI[b]
	DPPH scavenging activities	MAO-A	MAO-B	
3b	24.3 ± 5.1	8.7%[c]	31.2 ± 0.5	-
3d	15.4 ± 2.0	86.3 ± 2.1	6.4 ± 0.9	10.9
3f	29.1 ± 3.4	27.9%[c]	40.5 ± 2.4	-
5c	45.7 ± 0.8	50.1 ± 1.9	15.6 ± 1.8	3.2
Resveratrol[d]	104.3 ± 3.8	-	-	-
Ladostigil	-	-	36.2 ± 3.1	-
Selegiline[d]	-	67.2 ± 1.2	19.6 ± 0.8 nM	3429
Iproniazid[d]	-	6.5 ± 0.7	7.3 ± 0.4	0.9

[a]Each IC_{50} value shown in this table were the mean±SEM from three experiments.

[b]hMAO-B selectivity index = IC_{50}(hMAO-A)/IC_{50}(hMAO-B).

[c]The inhibition rate of compounds to MAO-A at 100μM.

[d]Resveratrol, selegiline and iproniazide were used as positive control.

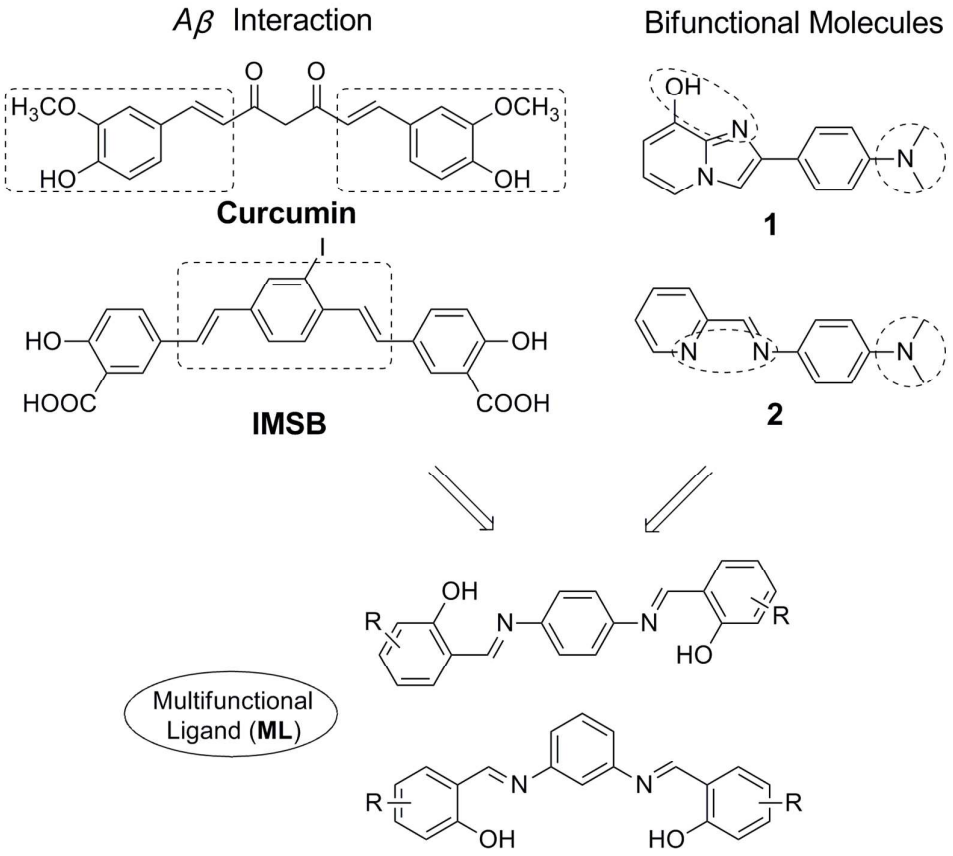
Aβ Interaction
Bifunctional Molecules
Curcumin
IMSB
1
2
Multifunctional Ligand (ML)

Fig. 1.

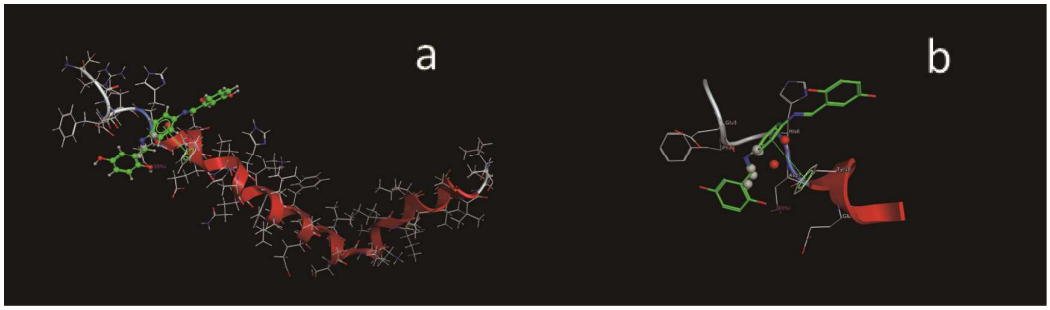
a
b

Fig. 2.

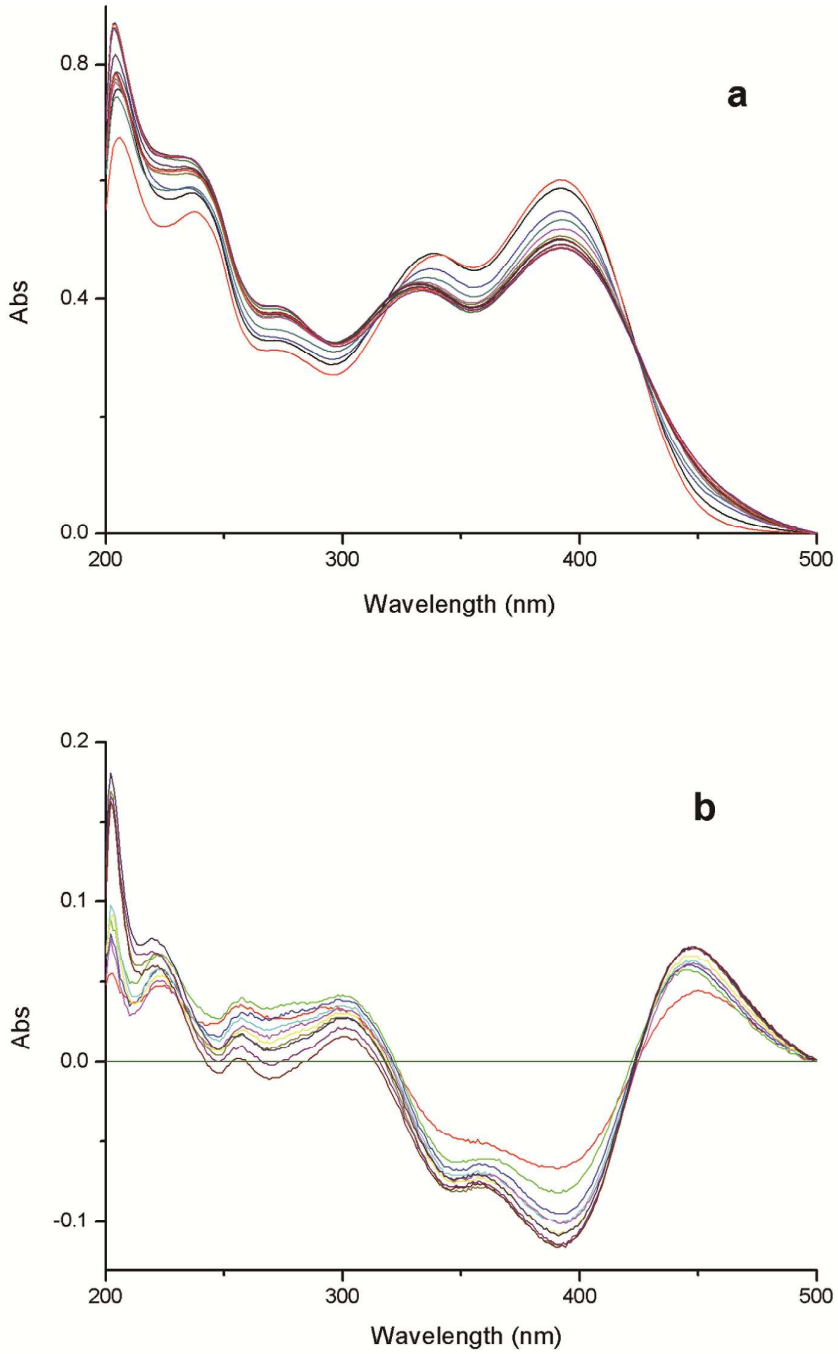
a
Abs
0.8
0.4
0.0
200
300
400
500
Wavelength (nm)
b
Abs
0.2
0.1
0.0
-0.1
200
300
400
500
Wavelength (nm)

Fig. 3.

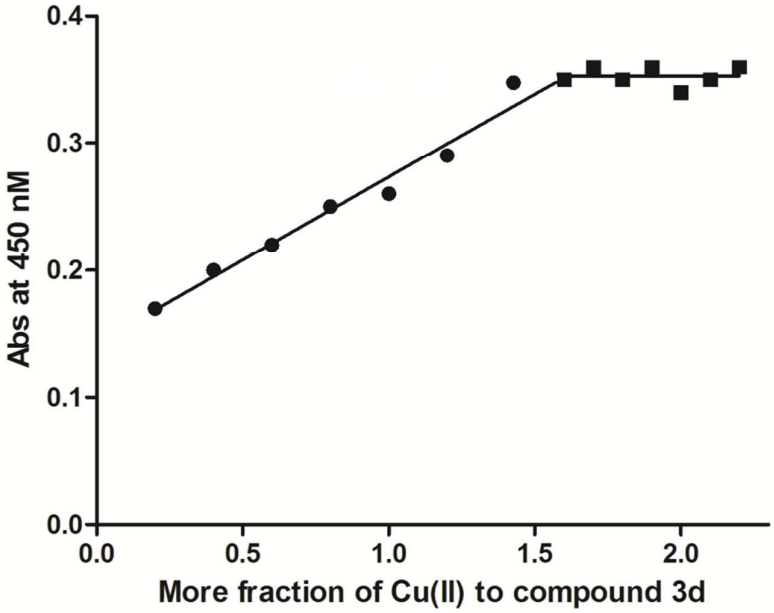
0.4
0.3
0.2
0.1
0.0
Abs at 450 nM
0.0
0.5
1.0
1.5
2.0
More fraction of Cu(II) to compound 3d

Fig. 4.

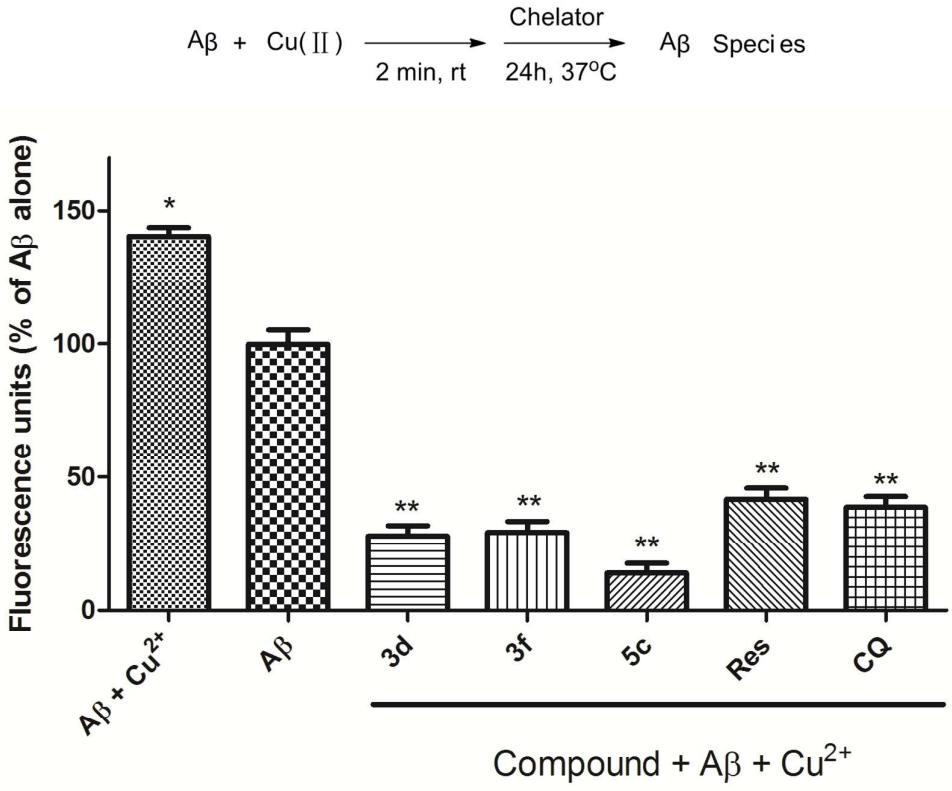
Aβ + Cu(Ⅱ)
2 min, rt
Chelator
24h, 37°C
Aβ Species
Fluorescence units (% of Aβ alone)
150
100
50
0
*
**
**
**
**
**
Aβ + Cu2+
Aβ
3d
3f
5c
Res
CQ
Compound + Aβ + Cu2+

Fig. 5.

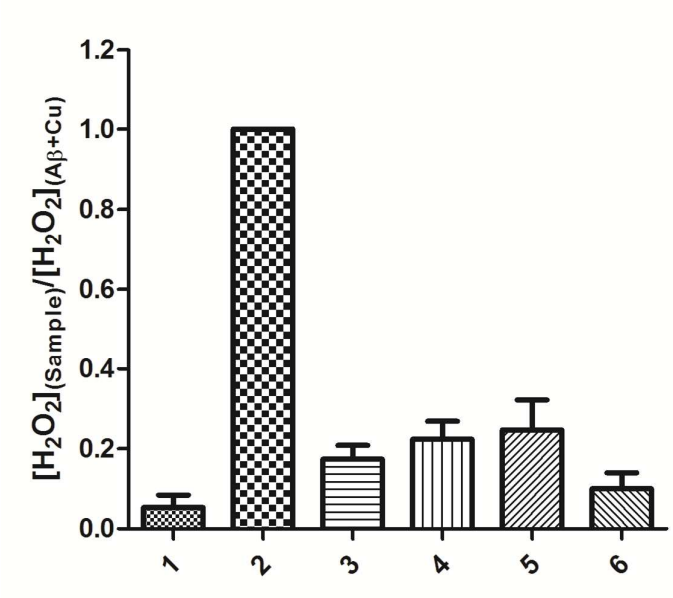
1.2
1.0
0.8
0.6
0.4
0.2
0.0
[H2O2](Sample)/[H2O2](Aβ+Cu)
1
2
3
4
5
6

Fig. 6.

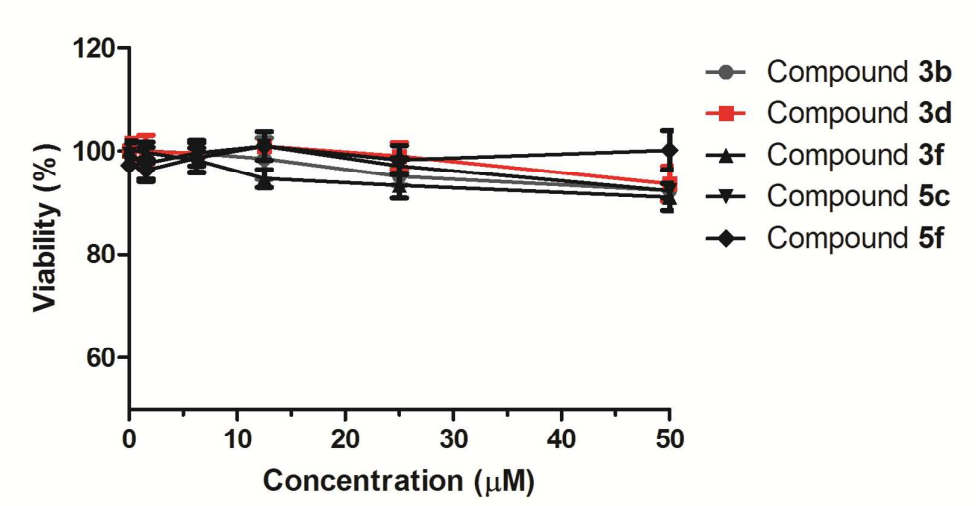
120
100
80
60
Viability (%)
0
10
20
30
40
50
Concentration (μM)
Compound 3b
Compound 3d
Compound 3f
Compound 5c
Compound 5f

Fig. 7.

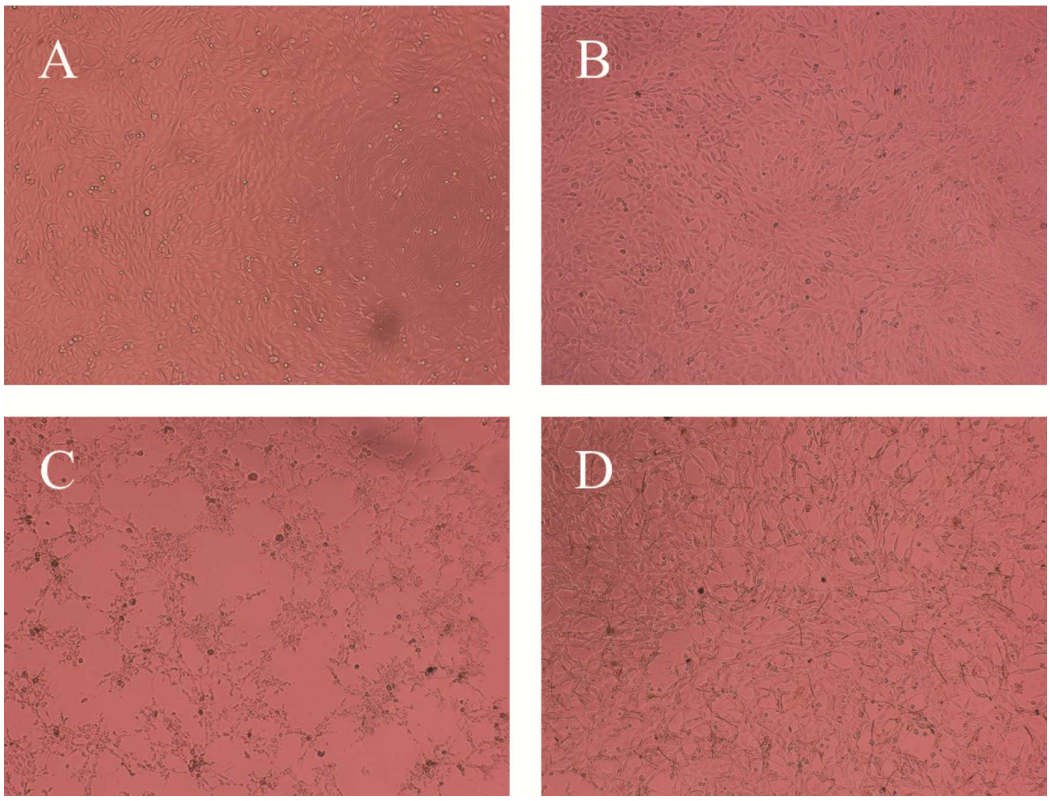
A
B
C
D

Fig. 8.

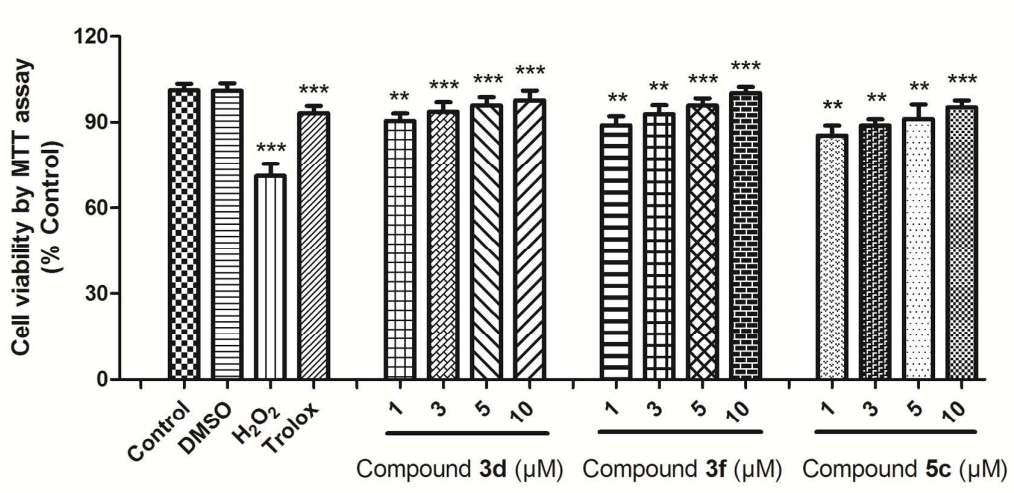
Cell viability by MTT assay (% Control)
120
90
60
30
0
Control
DMSO
H2O2
Trolox
1
3
5
10
Compound 3d (μM)
Compound 3f (μM)
Compound 5c (μM)

Fig. 9.

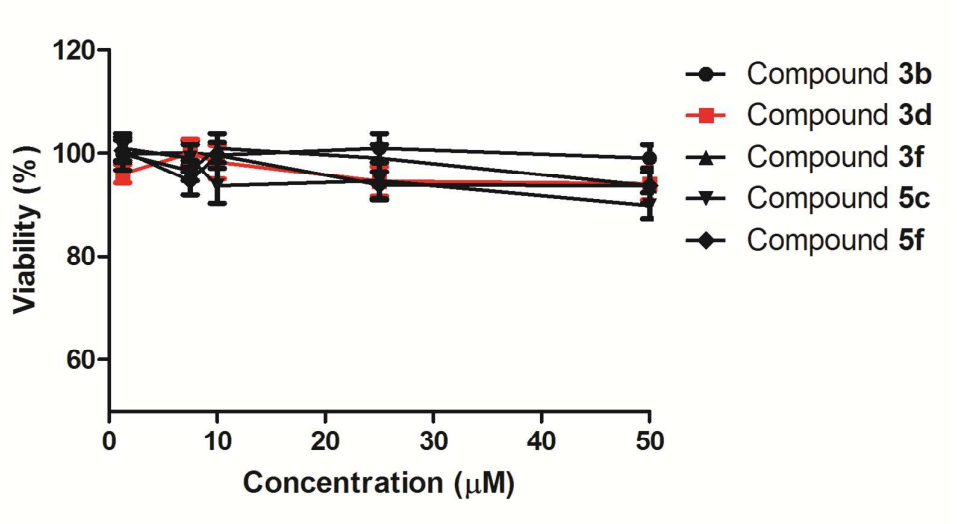
120
100
80
60
Viability (%)
0
10
20
30
40
50
Concentration (μM)
Compound 3b
Compound 3d
Compound 3f
Compound 5c
Compound 5f

Fig. 10.

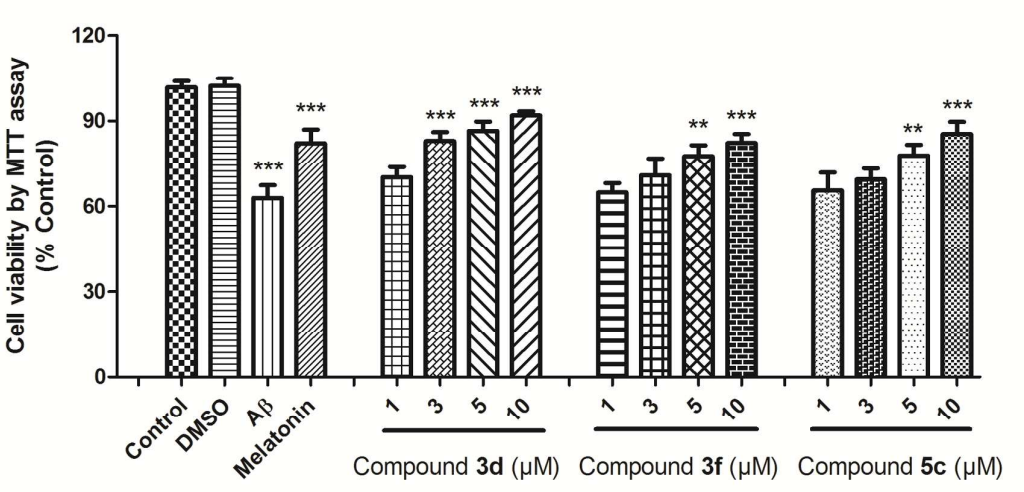
Cell viability by MTT assay (% Control)
120
90
60
30
0
***
**
Control
DMSO
Aβ
Melatonin
1
3
5
10
Compound 3d (μM)
Compound 3f (μM)
Compound 5c (μM)

Fig. 11.

Scheme 1.

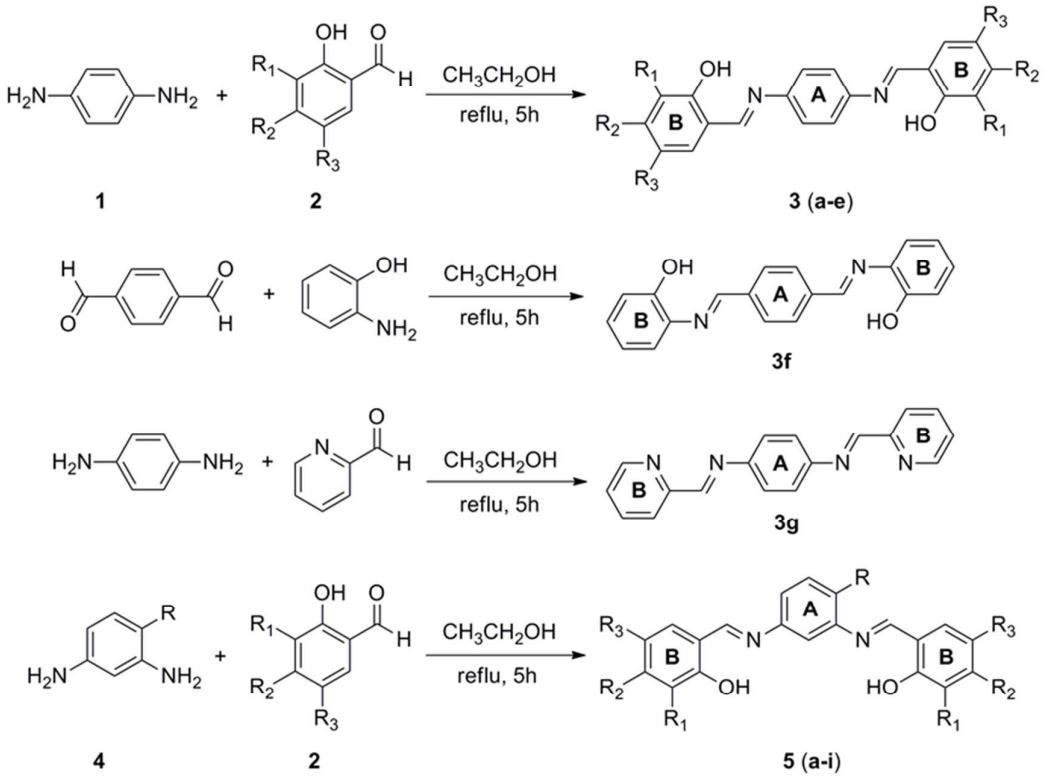

Compound	R	R_1	R_2	R_3
3a	H	H	H	H
3b	H	OH	H	H
3c	H	OCH_3	H	H
3d	H	H	H	OH
3e	H	H	H	OCH_3
5a	H	H	H	H
5b	H	OCH_3	H	H
5c	OH	OCH_3	H	H
5d	H	H	OH	H
5e	H	H	OCH_3	H
5f	H	H	$N(CH_3)_2$	H
5g	H	H	$N(CH_2CH_3)_2$	H
5h	H	H	H	Cl
5i	H	H	H	OCH_3